MASSACHUSETTS INSTITUTE OF TECHNOLOGY

APOLLO

GUIDANCE, NAVIGATION AND CONTROL

Approved: Albert P. Freeman
Albert P. Freeman
Deputy Associate Director
Charles Stark Draper Laboratory

Approved: David G. Hoag 19 May 72
David G. Hoag, Director
Apollo Guidance and
Navigation Program

Approved: Ralph R. Ragan 19 May 72
Ralph R. Ragan
Deputy Director
Charles Stark Draper Laboratory

E-2650

OIL-FILM-PARAMETER INVESTIGATION

by

Edward P. Kingsbury

April 1972

MIT CHARLES STARK DRAPER LABORATORY

CAMBRIDGE, MASSACHUSETTS, 02139

ACKNOWLEDGEMENT

This report was prepared under DSR Project 55-23829, sponsored by the Manned Spacecraft Center of the National Aeronautics and Space Administration through Contract NAS 9-4065.

E-2650

OIL-FILM-PARAMETER INVESTIGATION

ABSTRACT

A counter-rotating fixture was designed and built to measure starved EHD film thicknesses. Some good-geometry glass races were obtained. A theoretical analysis of starvation was made.

Measurements of retainer stability during "bimode" torque disturbances were made. The most common form of bimode was related to stability of retainer cock.

by

Edward P. Kingsbury
April 1972

TABLE OF CONTENTS

LIST OF ILLUSTRATIONS

OIL-FILM-PARAMETER INVESTIGATION

1. INTRODUCTION

This report covers effort under optical elastohydrodynamic (EHD) lubrication studies under contract NAS 9-4065 during calendar year 1971. Specific areas of emphasis during this reporting period were transparent-race experiments and retainer-motion studies.

2. TRANSPARENT-RACE EXPERIMENTS

2.1 Counter Rotation

Some measurements of EHD film thickness were obtained using the British glass races under flooded conditions, and reported last year.[1]* It was found difficult to get data at speeds above 3,000 r/min outer-race rotation (ORR) due to variable cross curvature in those races. Since the ten sapphire races also showed poor geometry (of a different kind) it was felt that conversion to counter rotation would be useful. In this mode, the races turn in opposite directions so that the ball group does not orbit. Thus each ball center is stationary, keeping any desired ball/outer-race contact position always in the microscope field. If the contact is lit with a stroboscope at the outer rate, only one position of the outer race is illuminated, so that race-geometry errors do not blur the contact image.

Accordingly, a counter rotation fixture (CRF) (Fig. 1) was designed, built, and run, using the British variable-curvature glass race on which the data of the previous report was obtained. This race originally had a 4-microinch bias coating, which had been partially worn off. Films were observed which had the same speed characteristic as previously reported in ORR: an abrupt initial buildup at lower speed, constant thereafter.

* Superscript numerals refer to similarly numbered references in the List of References.

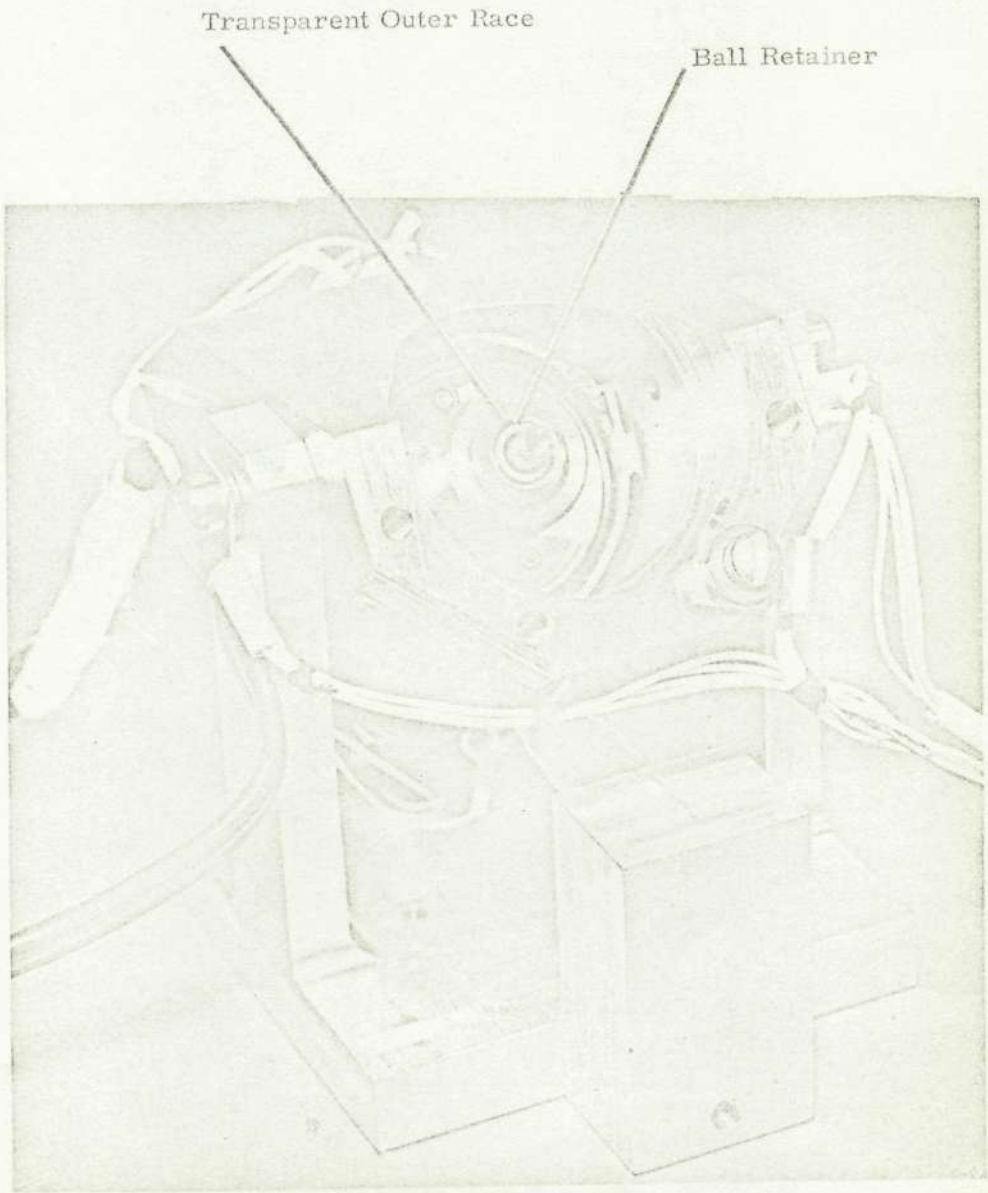

Fig. 1. Counter rotation fixture.

It was hoped to use the sapphire races in this fixture, but some trials showed the lobing of these races (owing to single crystal anisotropy) produced very rough running, so that milliwattmeter data was meaningless. A subcontract was placed with MPB to furnish ten new glass races with good groove geometry, which would also be round. These races, showing good inspection reports (Fig. 2), became available at the end of the year.

2.2 Semireflective Coatings

A capability for producing a semireflecting chromium layer inside the groove of the transparent races has been developed in-house. The method is sputter deposition, allowing the races to be ion-cleaned just prior to coating. Uniform layers of controllable density can be easily obtained. Preliminary experiments suggest that these layers will have the same life as those obtained from England. Figure 3 shows a typical stationary Hertz contact in a sapphire race coated by this technique.

2.3 Temperature Measurements

Since the retainer is stationary in counter rotation, it can be instrumented. A small thermocouple was embedded in the web between two ball pockets to follow temperature change (Fig. 4). In preliminary runs (with KG80), a temperature increase in the web of about 20°F over ambient was observed. Web temperature increased with speed, with dynamically stored bulk oil, and with time of running at constant speed (Fig. 5). The first two results suggest viscous drag as the source of friction between balls and retainer (rather than Coulomb friction). The last result, which was obtained using a sapphire race, seems contradictory, since the dynamically stored oil is expected to be depleted, and hence viscous drag to be reduced, with running. It may have been a result of the variable ball loading with the lobed race.

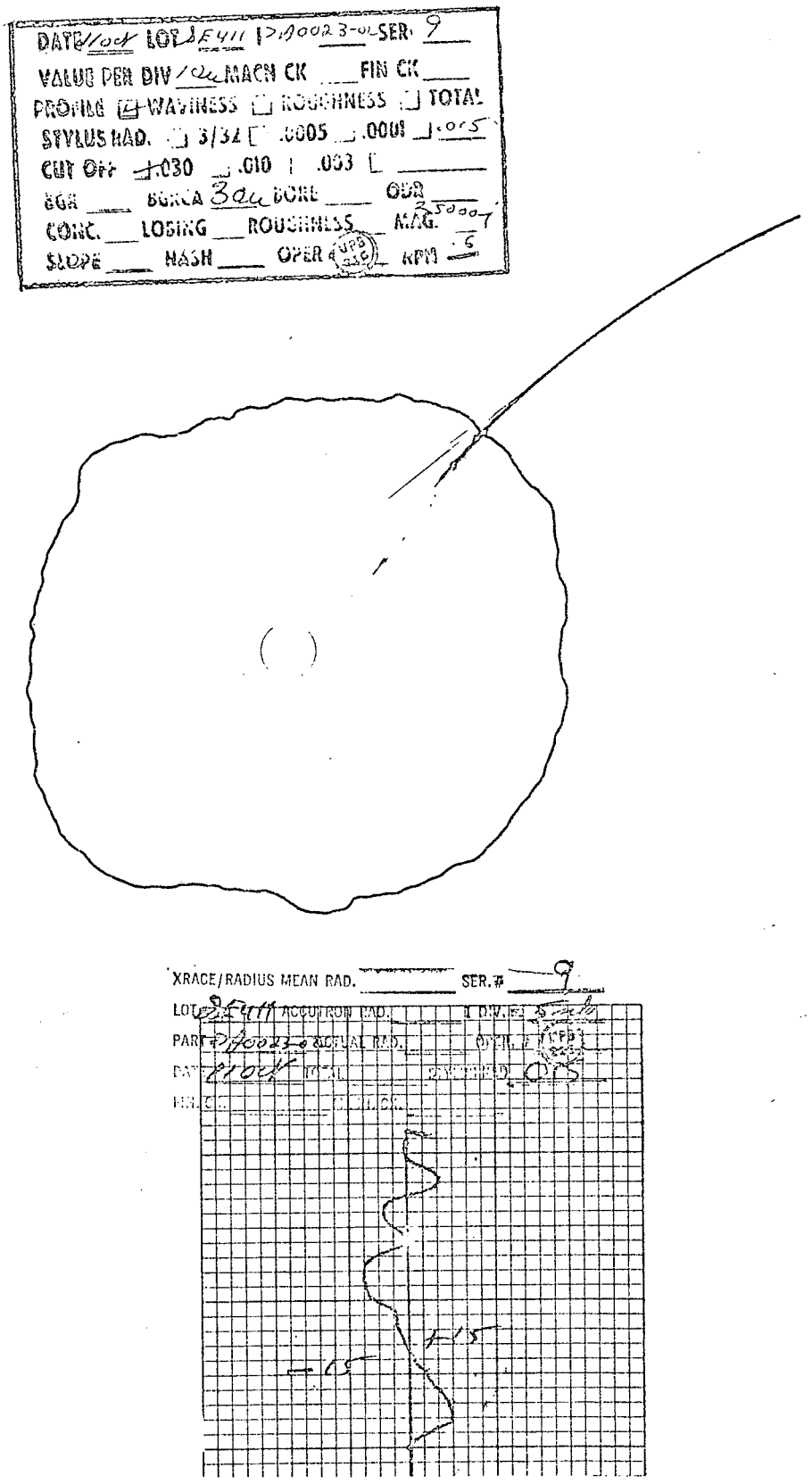

Fig. 2. MPB inspection reports.

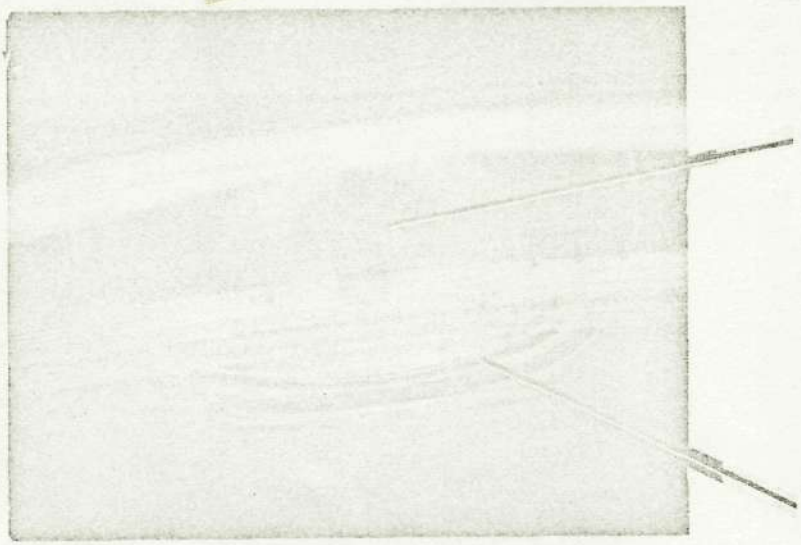

Fig. 3. Hertz zone in MIT sputter-coated sapphire race.

Fig. 4. Thermocouple in retainer.

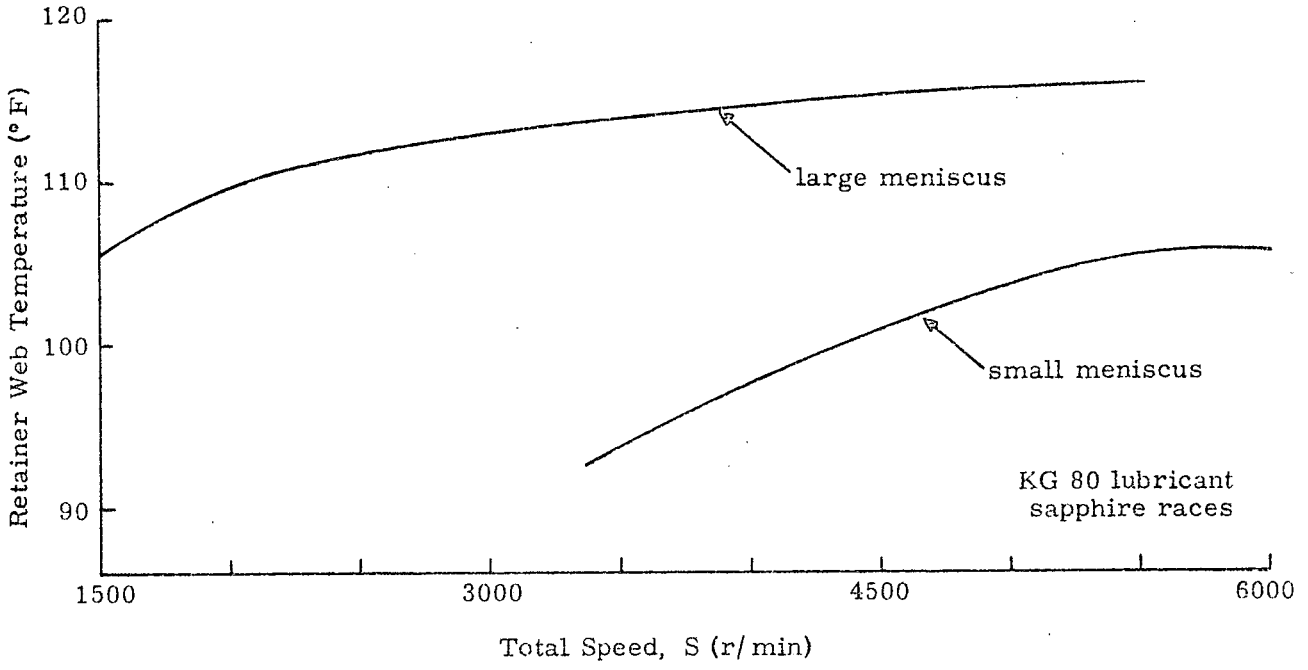

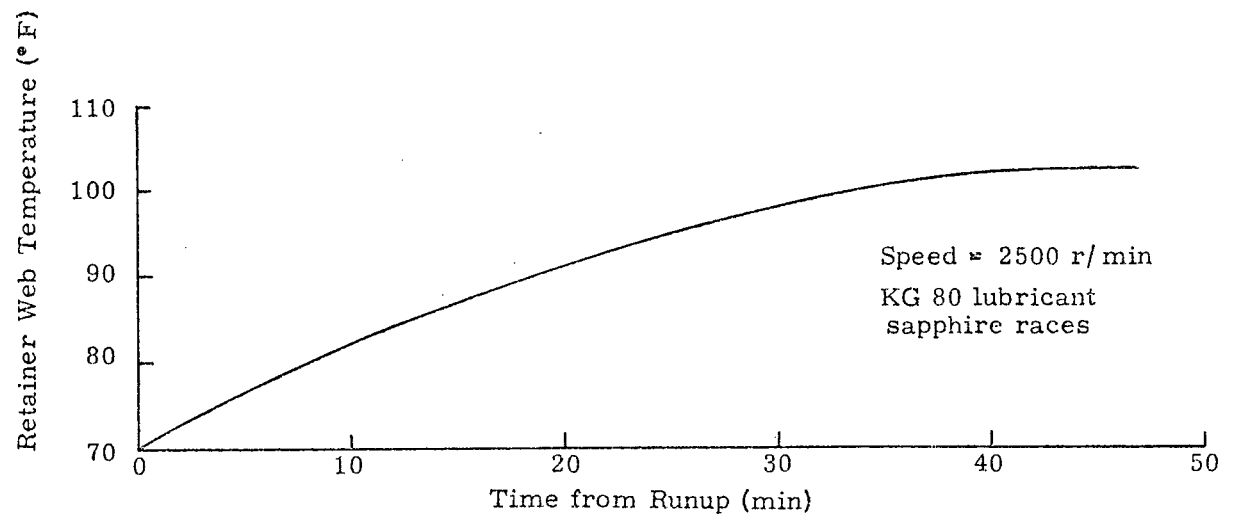

Fig. 5. Retainer web temperature vs speed and time after runup.

2.4 Dynamic Oil Storage

The amount of bulk oil dynamically stored (i.e., not in the retainer) can be calculated from the dimensions of the pool around the ball as seen through the outer race with the wheel at rest. Following Hertz[2], consider the gap g between the doubly curved surfaces of the ball and outer race as given by a quadratic in x (the roll direction) and y (the transverse direction):

$$g(x, y) = \frac{x^2}{2R'_x} + \frac{y^2}{2R'_y} \tag{1}$$

where

$$\frac{1}{R'_x} = \frac{1}{R_{\text{ball x}}} + \frac{1}{R_{\text{race x}}} \tag{2}$$

$$\frac{1}{R'_y} = \frac{1}{R_{\text{ball y}}} + \frac{1}{R_{\text{race y}}}$$

The gap is constant along the ellipses defined in Equation (1); in particular, at the edge of the oil pool, which has a measured half-width in the roll direction X:

$$g(X, 0) = \frac{X^2}{2R'_x} \tag{3}$$

The volume of stored oil for a measured X is thus (Fig. 6)

$$v = 4\int_0^X \int_0^{\left[\frac{R'_y}{R'_x}(X^2 - x^2)\right]^{1/2}} \int_0^{\left[\frac{x^2}{2R'_x} + \frac{y^2}{2R'_y}\right]} dg\, dy\, dx = \frac{\pi}{4R'_x}\sqrt{\frac{R'_y}{R'_x}}\,(X^4) \tag{4}$$

If the half Hertz width X_H is not small compared to X, a correction to v can be made by subtracting out the corresponding Hertz volume.

For the Apollo bearing, per contact:

$$v = 22.4\, X^4 \text{ cm}^3, \text{ if X is measured in cm.}$$

For a 7-ball Apollo bearing, assuming the inner contact to store the same amount as the outer:

$$v = 314\, X^4 \text{ cm}^3$$

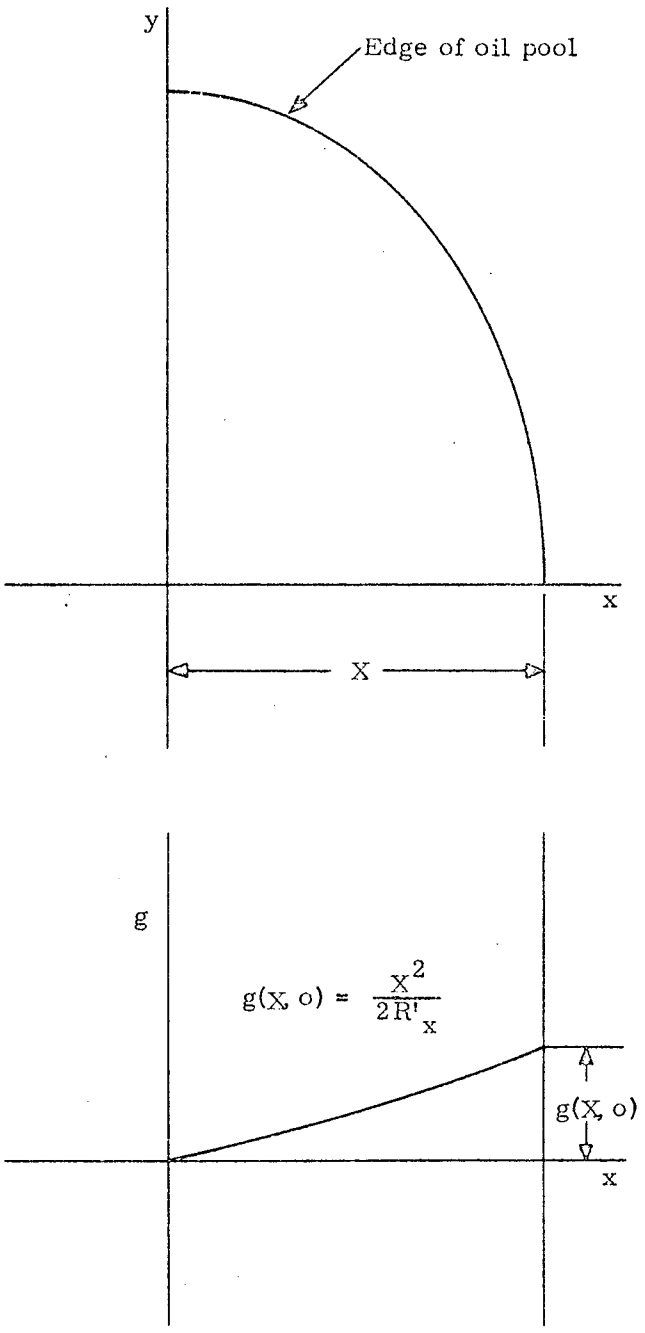

Fig. 6. Oil pool geometry.

The top part of Fig. 7 compares the oil pool found right after running a low-oil-temperature test with that found 12 hours later. About 50 times as much oil as initially present on rundown has been drawn to the contact during the 12 hours. The lower half of Fig. 7 makes the same comparison for a high-oil-temperature test. There is about 200 times as much oil as in the low-oil-temperature test, and no noticeable slow flow to the track.

2.5 Surface Tension

The oil pools in Fig. 7 are formed because the fluid oil is drawn into the small clearances near the Hertz zone and is held there by surface-tension forces. Some experiments were run to see how much distortion of the pool occurred due to the centrifugal field associated with retainer rotation. The whole wheel assembly was rotated as a solid body at 300 Hz using the inner-race motor and support bearing, in the counter-rotation fixture. This produced a three-halves larger centrifugal acceleration than the 243-Hz retainer rate of standard Apollo operation. Figure 8 compares the shape of the pool when stationary and when under the 1380-g acceleration. Some oil has moved to the unloaded side of the track (further from the spin axis), but the surface-tension forces still retain a large volume of fluid oil on the unfavorable side of the contact. The pictures are of an "F" type outer race.* Some of the new MPB glass races have been ground to produce "R" geometry. It is expected that pools formed on R races will not be able to retain so much oil on the uphill side of the contact.

The importance of surface tension in determining oil distribution in the small clearances around the Hertz zone, particularly in the starved case, is demonstrated both by the preceeding experiment and by experiments of Cameron[3]. In fact, Cameron suggests that the surface tension of the

* F stands for full groove, R for relieved groove. In bearing manufacturer's terminology, a B bearing has an R inner and an F outer; an H bearing has an F inner and an R outer.

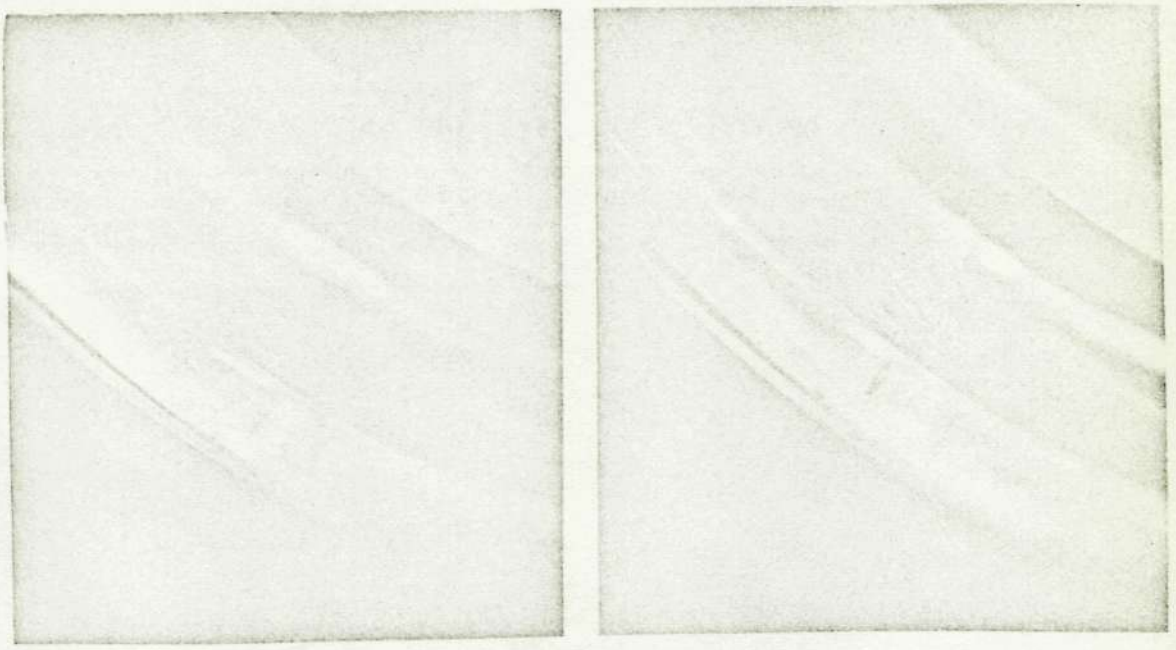

LOW OIL

ON RUNDOWN

12 HOURS LATER

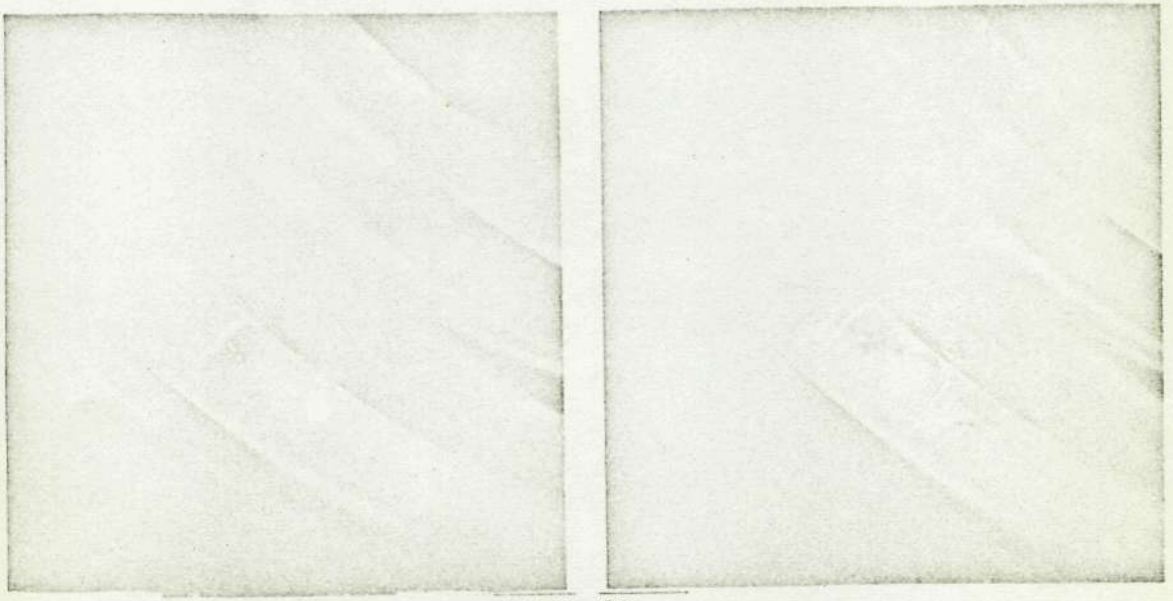

HIGH OIL

ON RUNDOWN

12 HOURS LATER

Fig. 7. Low and high oil pools.

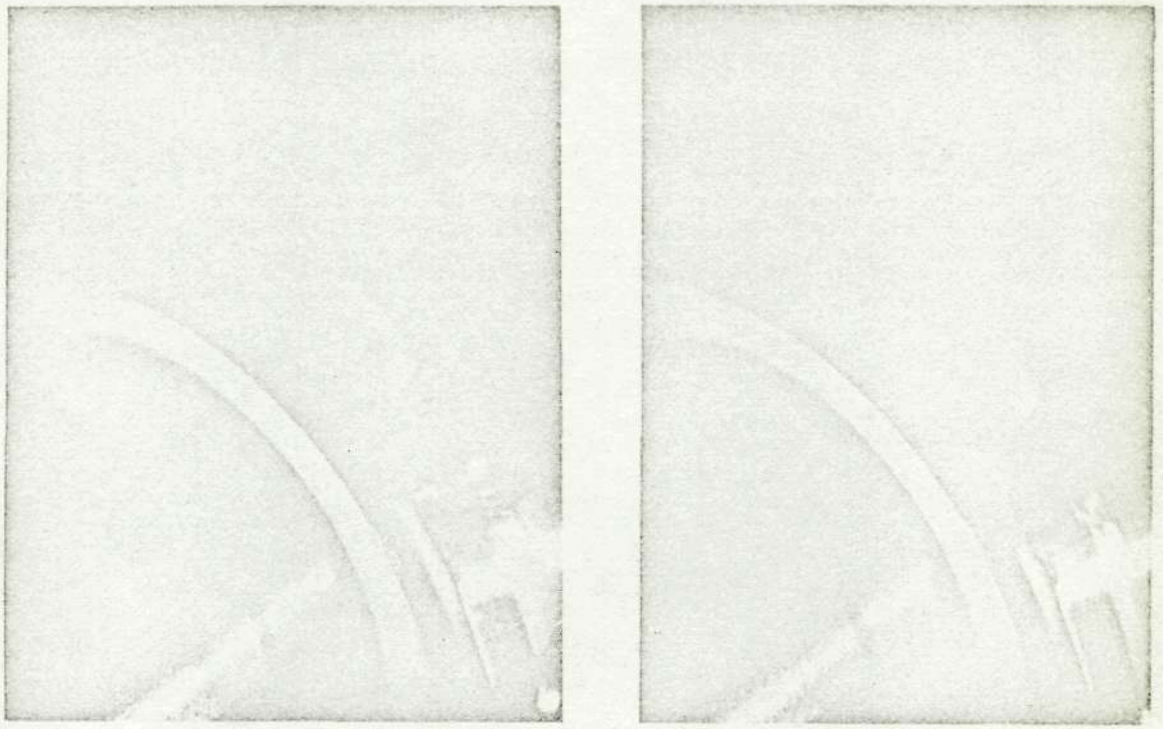

at 1 g

at 1380 g's

Fig. 8. Oil-pool-shape variation with g.

lubricant is a more important parameter for starved EHD calculations than load or speed. With this in mind, Wedeven[4] has measured surface tension of some fluid candidates for EHD application. Similar measurements can be made by supporting liquid drop on a hydrodynamically established film of air[5]. The drop shape is a measure of its surface tension[6]. The advantages of this method are: a measurement may be made on almost any liquid without regard for liquid-solid interactions, only a very small amount of liquid is required, and the relative effect of additives or temperature can be easily obtained. Figure 9 compares the shape of a drop of KG 80 before and after being contaminated with a trace of silicone fluid (which lowers its surface tension).

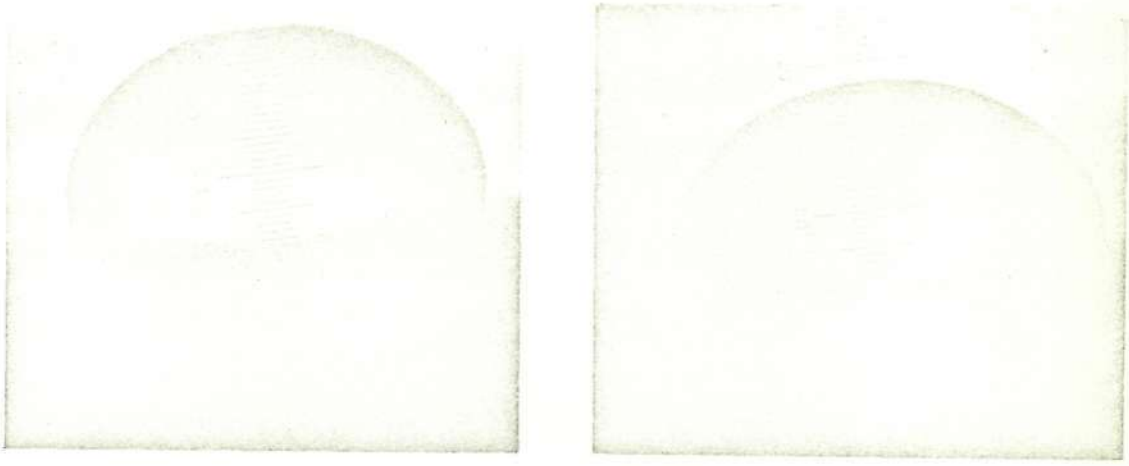

KG 80 oil

KG 80 oil contaminated with silicone fluid

Fig. 9. Oil-drop shape.

2.6 Film-Thickness Calculations

The salient feature of starved EHD lubrication is that there is not enough oil available to produce the complete film contemplated by Reynold's equation. Modifications to the classical EHD type of solutions therefore are not really applicable to a starved contact. With this in mind, a calculation of film thickness was undertaken from the point of view that more oil available at the contact should increase the film thickness. The details of this calculation are given in the appended paper, "Cross Flow in a Starved EHD Contact," to be presented to the ASLE. Briefly, consider that there is a circulation of oil within the bearing, into and out of a volume having the lateral dimensions of the Hertz zone, and the oil-film thickness. The outflow is easily computed for a given thickness; for equilibrium an equal inflow must be provided. This approach allows life, flow rates, and jag decays to be estimated. As an example, for the Apollo configuration using SRG 160 at 130°F, to maintain a 5-microinch film, 7×10^{-2} μ gm/hour flow to the track is calculated.

The analysis seems to give reasonable numbers for known situations, but since some questionable simplications have been made, a direct experimental check is desirable. The MIT jag gun is being used to throw known masses of oil into a full-ball-complement bearing running on the Northrop film gage. Thus an average flow required to keep the film constant can be obtained. These experiments are in progress.

3. RETAINER-MOTION STUDIES

3.1 Bimodes

The Apollo package often shows large abrupt shifts in driving torque from one stable level to another. The shifts are back and forth between two definite levels, hence the name "bimode". Occasionally one positive shift is followed by another to give a "trimode". The shifts are uniform in amplitude, and the total torque remains between 1000 and 3000 dyne-cm. The shifts in torque correlate with changes in SRA unbalance, leading to speculation that changes in EHD film thickness are involved. But cross-flow analysis suggests that a sudden drop in film thickness (corresponding to a negative torque shift) is impossible.

As an alternative, the torque shifts could be due to abrupt changes in the average motion of either or both ball retainers. Drive-torque steps would be produced by different wedging or braking-force systems between retainer and balls/race; the SRA unbalance by an axial shift of the retainer CG when its average motion changes. Some indication that the torque shifts are accompanied by changes in retainer motion had come from stroboscopic observation. It was decided to adapt an existing optical probe system to see if a less subjective observation of Apollo retainer motions could be made, and if the torque shifts could be associated with them.

3.2 Measurement of Retainer Motion

A measure of the retainer motion in each bearing of a pair is obtained by focusing a light on the retainer's face and monitoring the reflected

light with a photocell into a dual-beam cathode-ray-oscilloscope (CRO) (Fig. 10). This setup was originally intended for use with a retainer guided on two inner-race lands, which cannot cock. A sinusoidal output from the photocell then corresponds to a radial motion of the retainer edge due to eccentric whirling. The Apollo retainer rides on only one land and might cock through substantial angles. A sinusoid appearing on the scope could then be produced either by cocking or by whirling (Fig. 11), or by a combination. In most of the data reported here, this ambiguity is present; although recent experiments suggest that the sinusoid should be interpreted as cocking rather than whirling. Rotation of the retainer is measured with a nonreflecting mark on the retainer surface, which gives a spike riding on the sinusoid once each retainer revolution.

Figure 12 is photographs of the photocell outputs on the CRO in an assembly where both retainers have stable rotations, forwards and backwards. The retainers are identified by their location at + or - SRA and the rotation as + or - according to the right hand rule at 243 Hz. The CRO sweep period is 0.02 second, showing five successive revolutions for both retainers in each photo. The stable criterion is that a retainer executes the same motion every time it rotates. The traces in Fig. 12 have this characteristic, sinusoids corresponding to to a cocking (whirling), with superimposed spikes corresponding to rotation, identical for all 5 revolutions in both bearings. Moreover, the two photographs are mirror images showing, in this assembly, that the sequence of retainer positions for - rotation is exactly the reverse of that for + rotation. This result gives confidence in the optical probe method.

3.3 Measurement of Driving-Torque Variations

The Apollo wheel was driven in air using a variable-frequency supply so that the nominal ball-group orbit frequency was 243 Hz. The power to one phase was recorded through a milliwattmeter. The traces show the variations in power (torque) after about 3.5 watts of friction, windage, and copper loss have been nulled out.

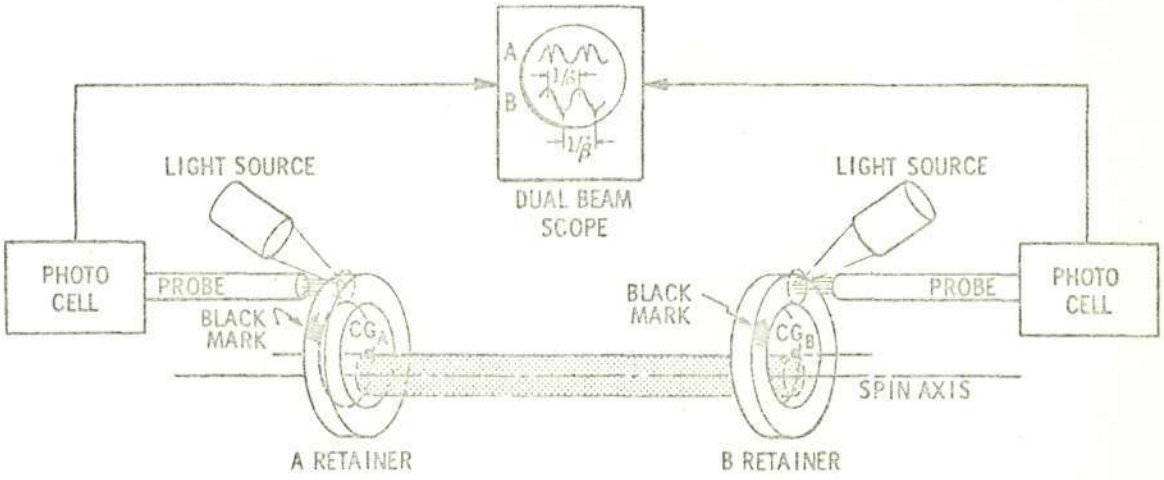

Fig. 10. Optical probe setup.

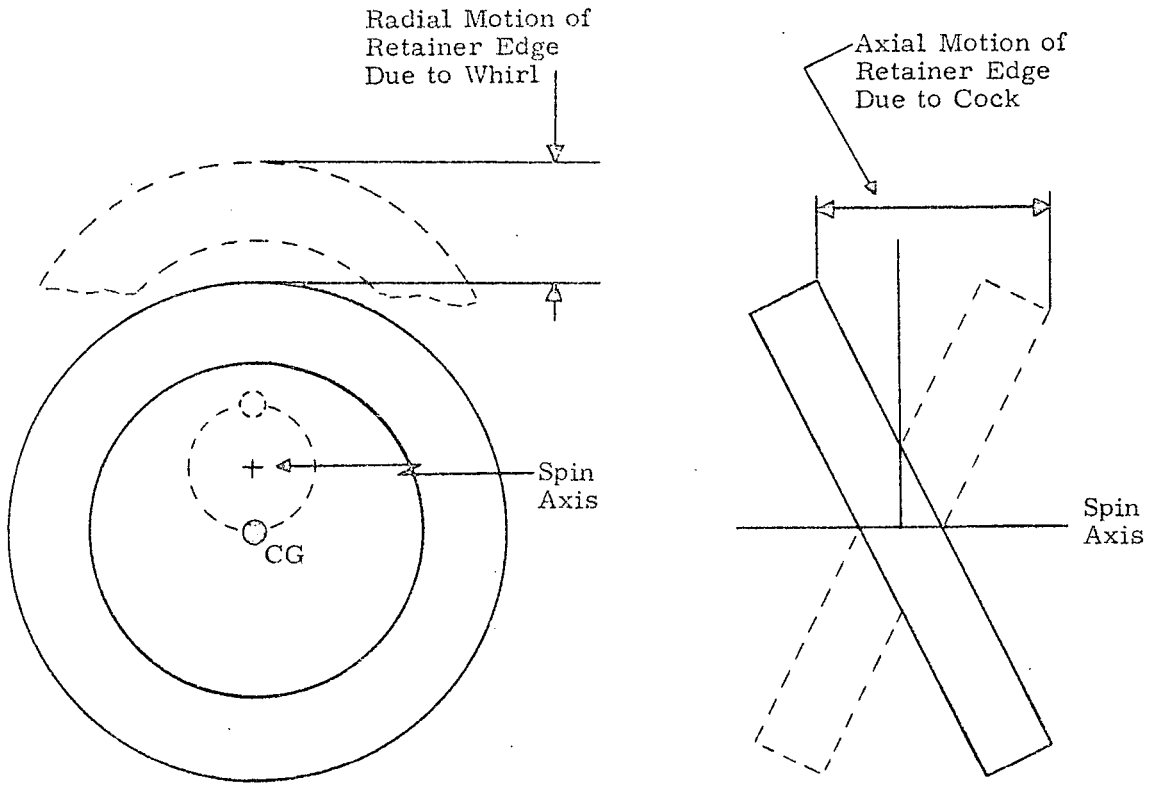

Fig. 11. Comparison of whirling vs cocking retainer motion.

Figure 13 compares a combination of positive and negative torque shifts with the classical oil jag. The bimodes show an abrupt shift (modified by the recording-system characteristic time) with a constant level between; the jags show an abrupt rise followed immediately by a long decay back to the original level. If the strip-recorder-paper speed is set too low, the distinction between jag and positive bimode, namely the immediate long decay in torque, can be lost, jags being misidentified as short bimodes.

+ Rotation

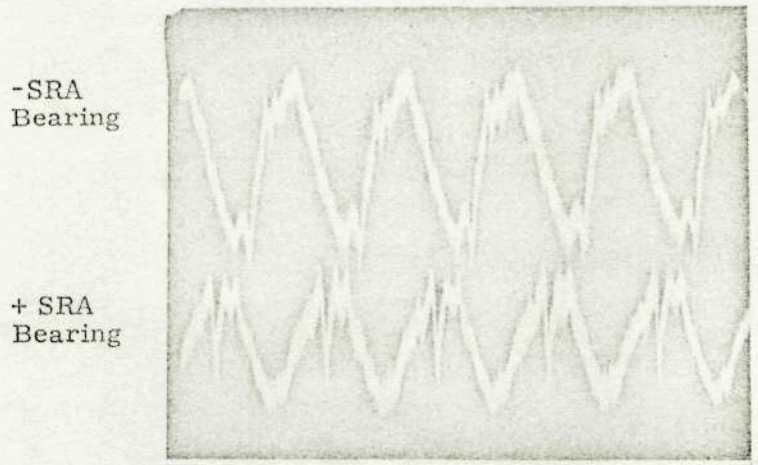

- Rotation

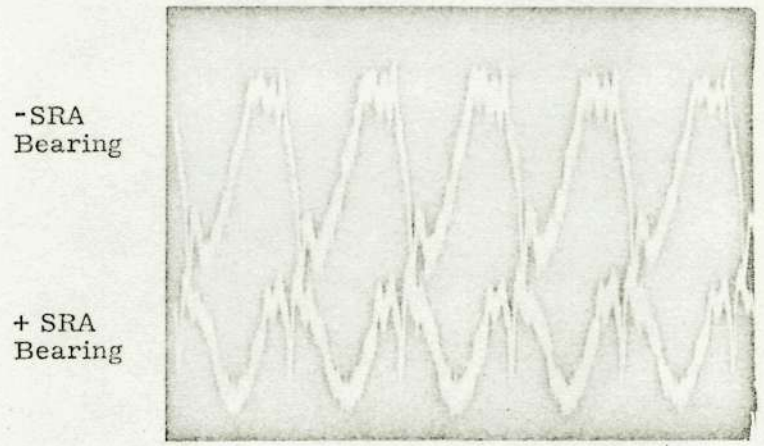

Fig. 12. Probe outputs for stable operation.

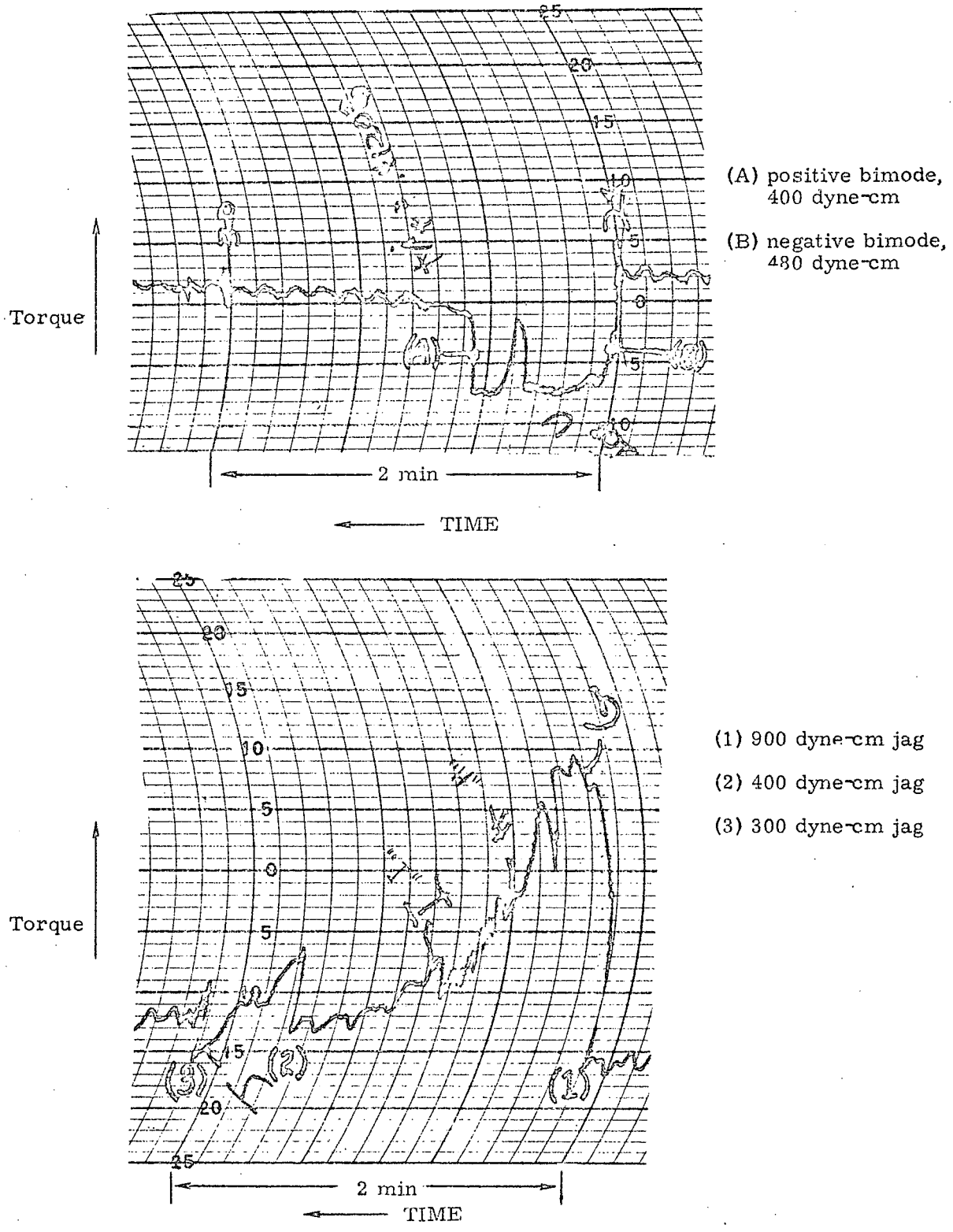

Fig. 13. Milliwattmeter traces showing bimodes and jags.

3.4 Bimode Retainer Instability

The optical probes show that the Apollo retainers rotate with a cocked axis during the high-torque part of the bimode. In Fig. 14, $\vec{N}$ represents a vector normal to the plane of the retainer face, cocked relative to the spin axis through the angle δ. As the bearing rotates, $\vec{N}$ traces out a cone of half angle δ at the ball-group orbit rate $\dot{\beta}$. For stable operation δ is a constant, δ_o. Consideration of clearances suggests that δ_o is about 0.6 degree, if there is no deformation of the retainer. During a torque bimode, it is found that the stability of one retainer suddenly changes. Figure 15 is a photo of the probe outputs during a torque bimode. The CRO sweep period for the top photo is 5 seconds showing about 1200 revolutions of each retainer. The + bearing is stable, the - bearing goes from unstable to stable. The lower photo is a sweep at 0.02 second showing the nature of the - SRA instability. The basic 243-Hz sinusoid is present but has random disturbances superimposed. Most of this sinusoid is due to eccentric whirl, since with unmodified retainers the probes do not distinguish whirl and cock. It will be shown later that when the retainer goes into a bimode instability, the cocking angle becomes small and variable. The driving torque demand accompanying the shift in retainer position is also

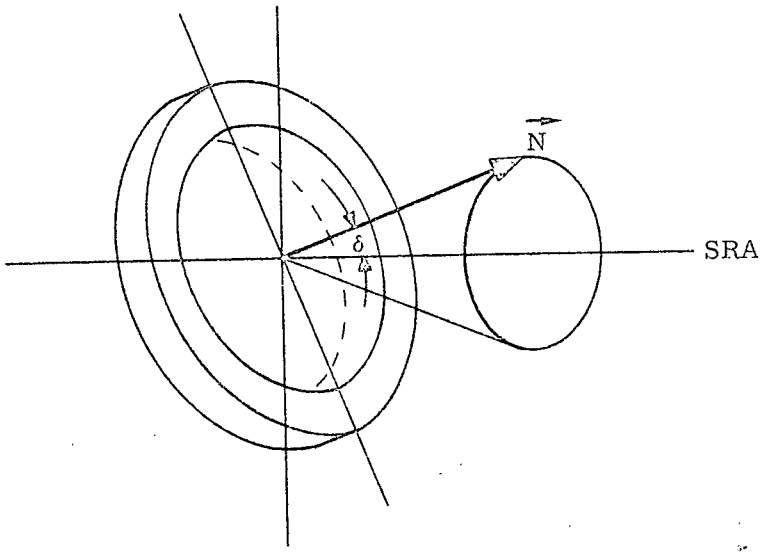

Fig. 14. Cocking geometry.

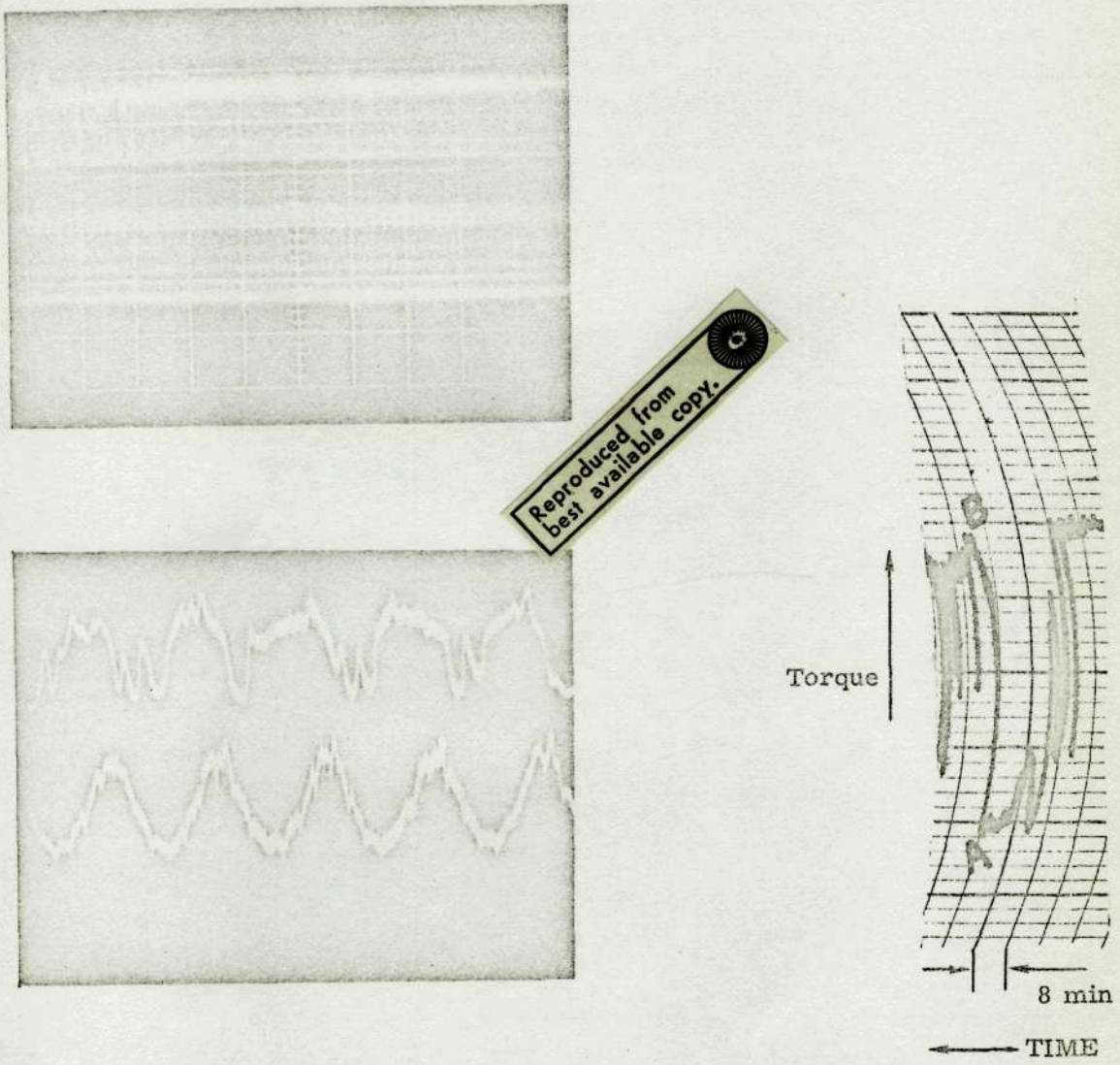

NOTE: Top trace in each photo is -SRA bearing.
Sweep in top photo is 5 seconds; in lower, 0.02 second.

Fig. 15. Probe output and milliwattmeter trace showing bimode.

shown in Fig. 15, occurring from A to B, a positive step of about 1000 dyne-cm. There are some shorter (and smaller) bimodes in Fig. 15 as well. Note that, in contrast with a jag, it takes about 4 minutes for the positive jump from A to B, although the change in retainer motion occurs in 1 revolution.

When a retainer is unstable, as in Fig. 15, a rattling or rustling noise comes from the running wheel. It is not particularly loud and would not be audible, even with a stethoscope, when the wheel is run inside a housing.

Evidence to show that the bimode torque shift is accompanied by a change in the cocking of one retainer was obtained by adding reflecting flanges to standard Apollo retainers, Fig. 16. A standard retainer may be compared in Fig. 4. The probes are positioned in the middle of the flanges so that they do not "see" either edge and are thus insensitive to whirl inputs. It was impossible to remove the whirl component completely, but Fig. 17 shows that it is small for a central probe position. That figure compares probe outputs on a - SRA retainer which runs cocked for + rotation and uncocked for - rotation. The 0.02-second-sweep-period traces show that the 243-Hz component is nearly absent from the - SRA probe output for negative rotation. The probe position was not changed for any of the photos in Fig. 17, hence the difference in amplitude for the - SRA signals either represents a change in retainer position from eccentric to central rotation, or a change from cocked to ordinary rotation. The latter interpretation is preferred since an eccentricity is seen only dimly by centrally placed probes, and central retainer rotation has never been observed in any ordinary bearing.

Further evidence comes from the fact that occasionally a bimode can be induced by moving the probe axially into contact (gently) with the outside face of a retainer which is showing a large stable sinusoid. This should have no effect on an eccentric whirl, but could trigger a change from a just barely stable cocked rotation. Figure 18 is photographs of central probe outputs, at D prior to an induction, and at E, just afterwards. The - bearing goes unstable, and

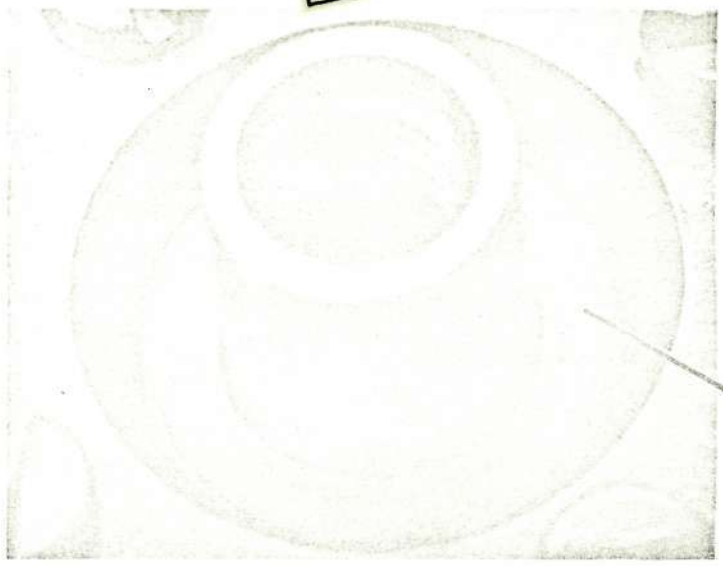

Fig. 16. Bearing with flanged retainer

the torque drops by 600 dyne-cm when the retainer face is touched. The + bearing remains unstable throughout.

Attempts to stabilize Apollo package performance against bimoding by stabilizing retainer motions (increased pendulosity and increased ball-group misalignment have been tried) lead to maximum driving-torque demands. In the case of ball-group misalignment coupling, for effective control the driving-torque requirement was very high. An experiment (suggested by Northrop) to remove bimodes by making the retainers always unstable was successful, producing a low uniform driving-torque condition. Small bumps of epoxy, measured as 0.003-inch high, were applied on both retainer guiding lands of an Apollo shaft. Figure 19 shows the probe outputs for this assembly. Both bearings show unstable uncocked rotations. There were no flanges on these retainers; hence they were not whirling either. The accompanying torque trace is at a low level, very uniform, and has a typical oil jag included. Apparently as the retainer inner-race contact hits the bump, the retainer is jolted into an uncocked central attitude. This happens 243 times each second, and the result is a typical unstable retainer motion requiring low torque. Even the rattling noise is produced.

+ Rotation – Cocked

– Rotation – Whirl

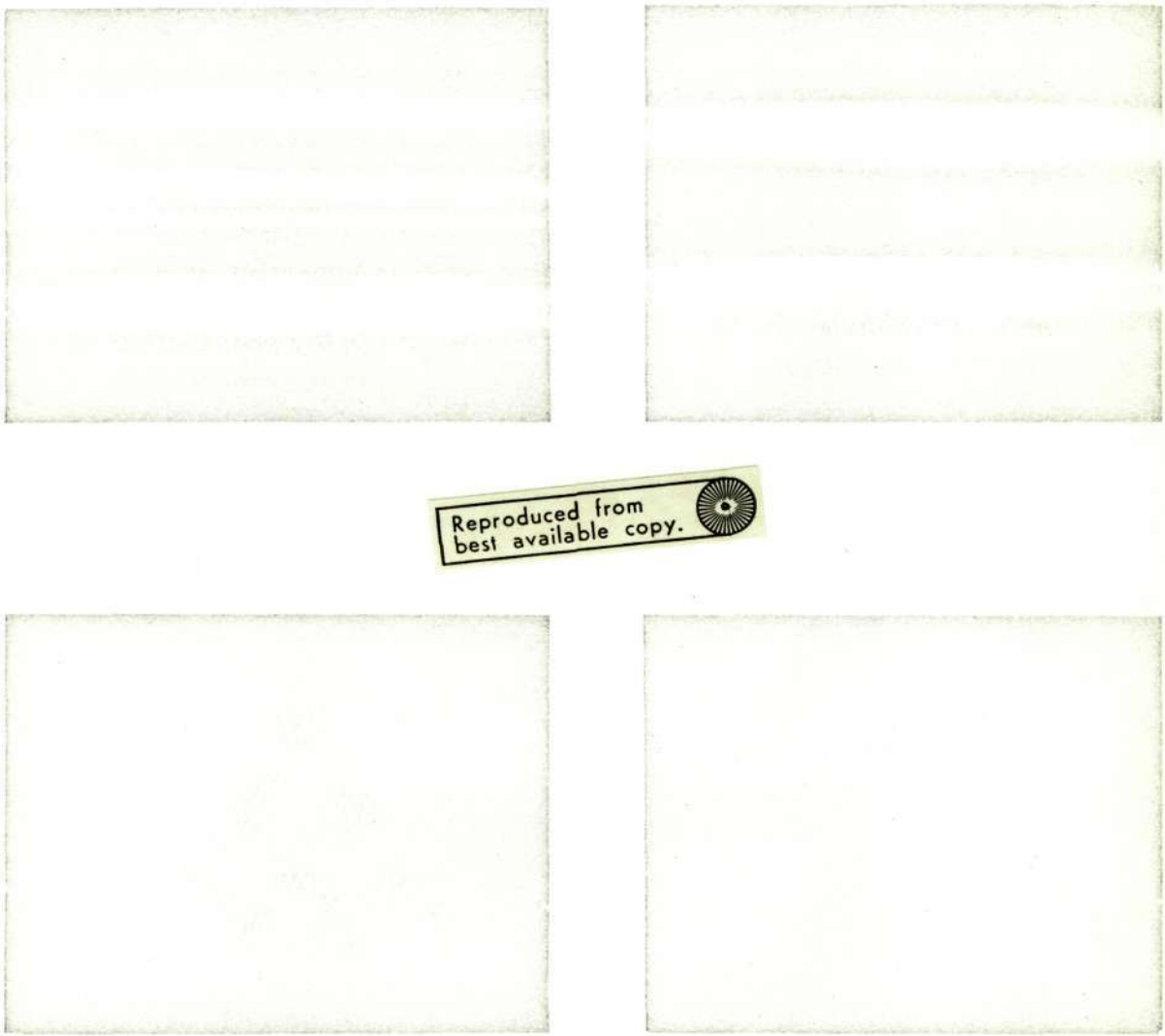

NOTE: Top trace in each photo is -SRA bearing.
Sweep in top photos is 5 seconds; in
lower, 0.02 second.

Fig. 17. + and - rotation for cock vs whirl.

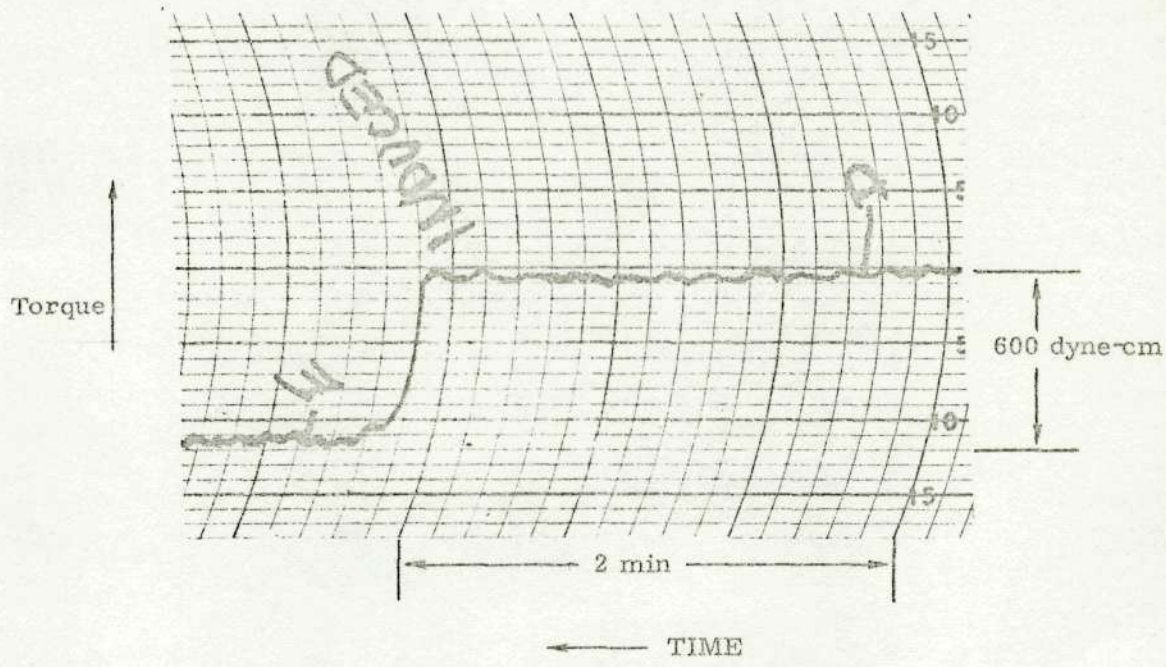

NOTE: Top trace in each photo is -SRA bearing; sweep is 0.02 second.

Fig. 18. Milliwattmeter trace and retainer motion during induced bimodes.

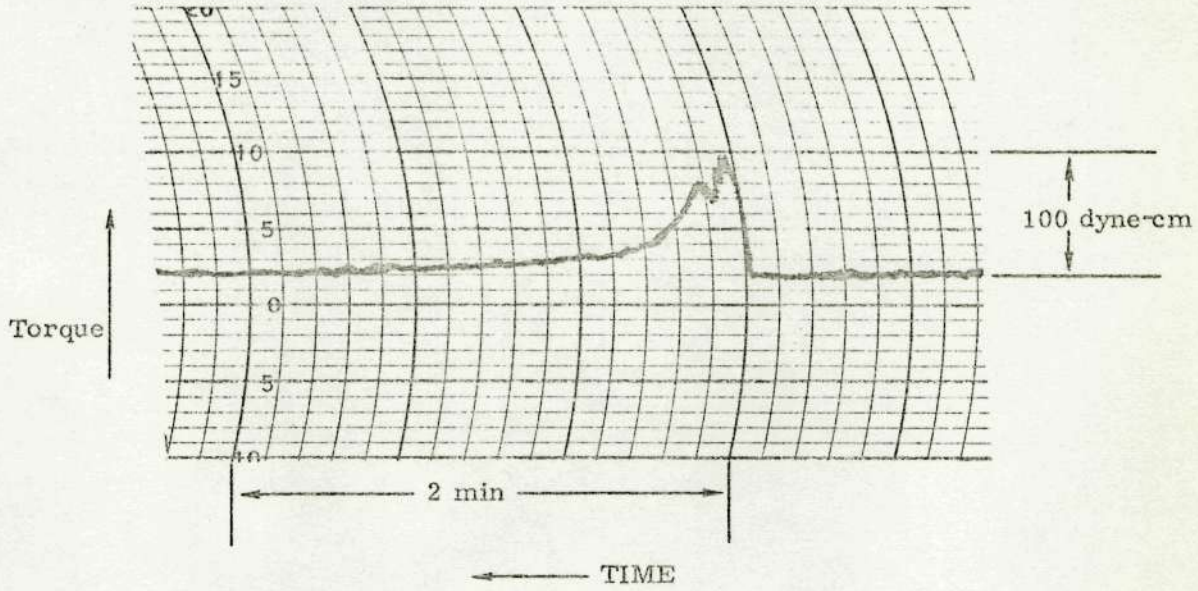

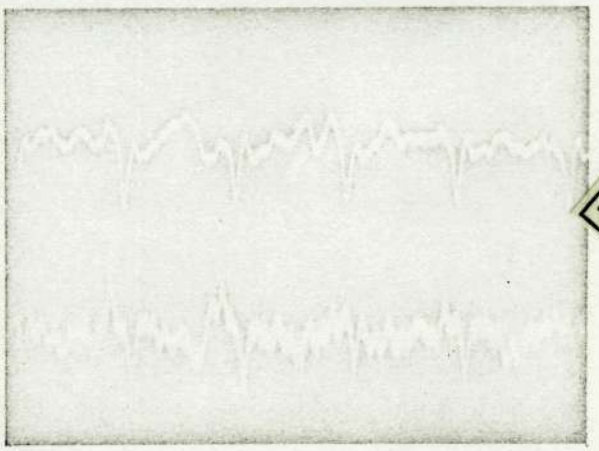

NOTE: Top trace in photo is -SRA bearing; sweep is 0.02 second.

Fig. 19. Milliwattmeter trace and retainer motion with bumpy land assembly.

3.5 Other Retainer Instabilities

In this program two wheels, four retainers, and four ball sets (three matched) have so far been run in different combinations. The tests show that the Apollo retainer can have a lot of different motions, some rather complicated. It isn't usually possible beforehand to predict which will be realized. In fact, the same assembly often shows different retainer modes on successive start ups or upon prolonged running. The classification of motion into stable and unstable is natural, but subclassification of unstable motions is more difficult. In this section, two instabilities of fairly simple character are discussed.

Figure 20 shows probe outputs during a "click" instability. The -SRA retainer suffers sudden random disturbances which last for one or two retainer revolutions. No torque change registers on the milliwattmeter, likely

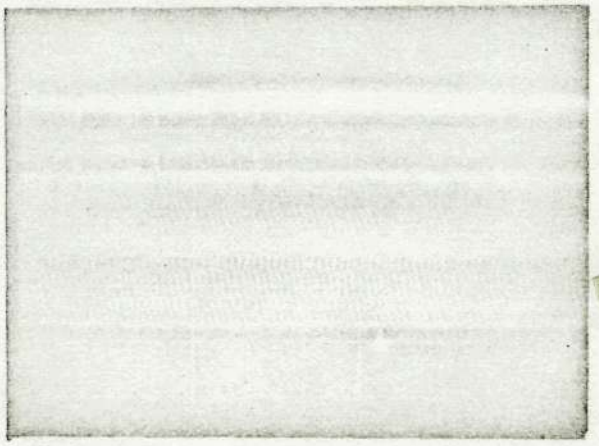

NOTE: Top trace is -SRA bearing; sweep is 5 seconds.

Fig. 20. Retainer motion during click disturbance.

due to a very short duration. These disturbances are probably very short negative-positive bimode pairs. Clicks can be heard when the wheel runs in air, but not with a stethoscope. The instability would not be picked up in ordinary wheel testing.

In another type of disturbance, the retainer undergoes spasms of a mild instability producing an audible rattle and a slightly decreased torque demand. The torque trace, Fig. 21, shows the demand when both retainers are stable, at A, terminated by a small oil jag. The onset of instability in the - SRA retainer is shown at B. The oil jags were a regular feature of this particular assembly and continued uninfluenced by the - SRA retainer stability throughout the run. Measurements of the + SRA ball-group rate showed a very slight decrease, about 0.05 Hz, during the jags, locating them in that bearing.

The probe outputs in Fig. 21 show first the behavior of the - SRA retainer when stable, and then a succession of different retainer motions (flips) which were seen during the instability. The changes in motion take place gradually, over many seconds, in a definite sequence of irregular duration. The rotation-locating spike moves with respect to the cock sinusoid. This means that $\vec{N}$ is moving with respect to the retainer. When the sequence carries the sinusoid back to its stable form, the torque reverts to the higher level and the rattling noise stops.

The torque trace prior to A is an example of a regular driving torque sinusoid and is a result of a bearing-bearing interaction due to ball-group misalignment. The period of this sinusoid is equal to the beat period of the two ball groups, in this case 8 seconds. A slight instability in the - SRA retainer accompanied one part of this cycle as well. This is shown in Fig. 22, which has a sweep period of 20 seconds, making each grid division equal to 2 seconds. The - SRA instability shows up as a slight broadening of the trace every 8 seconds corresponding to the retainer beat period as measured on the torque trace, and also directly by timing the phasing of the probe outputs. A faint rattle could be

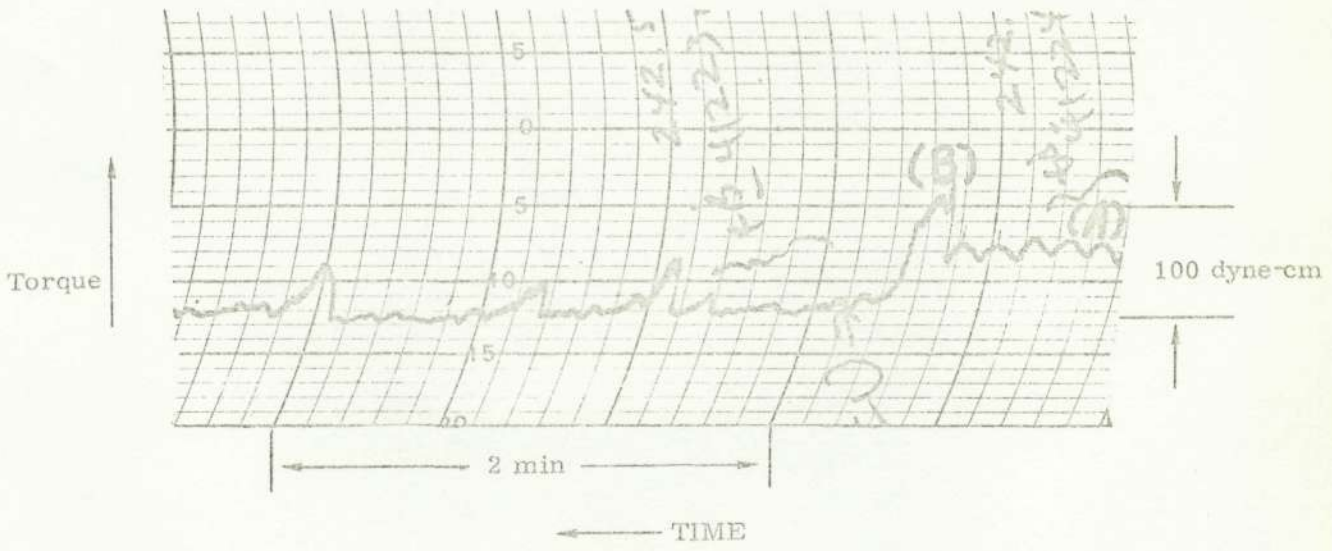

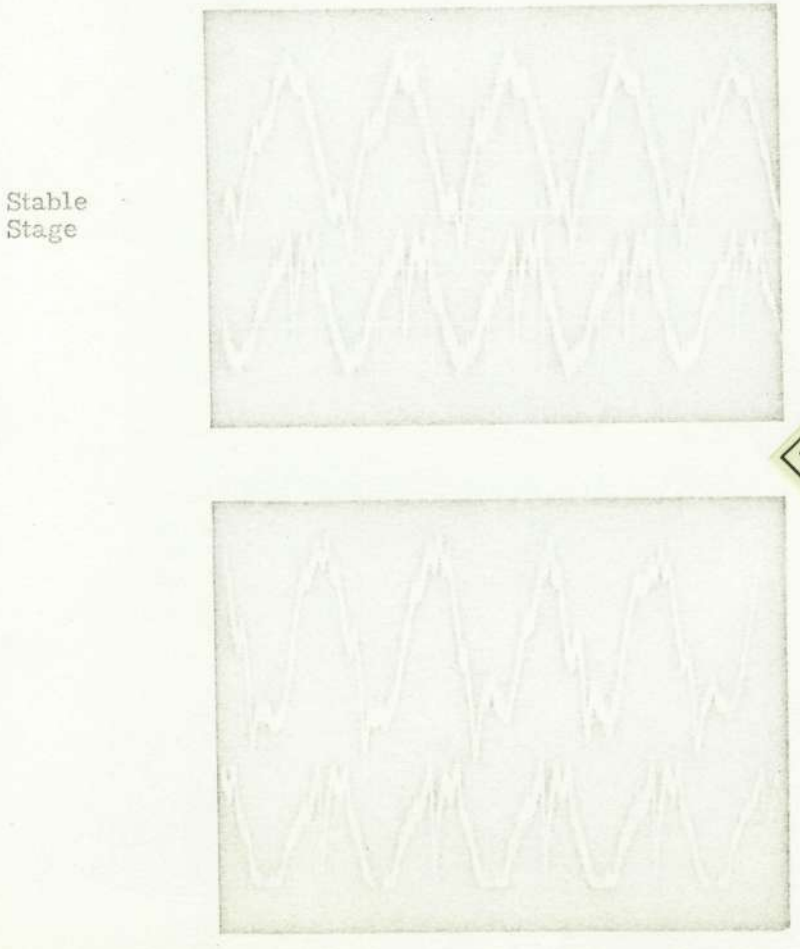

Fig. 21. Milliwattmeter trace and retainer motion during flip disturbance.
(Sheet 1 of 2)

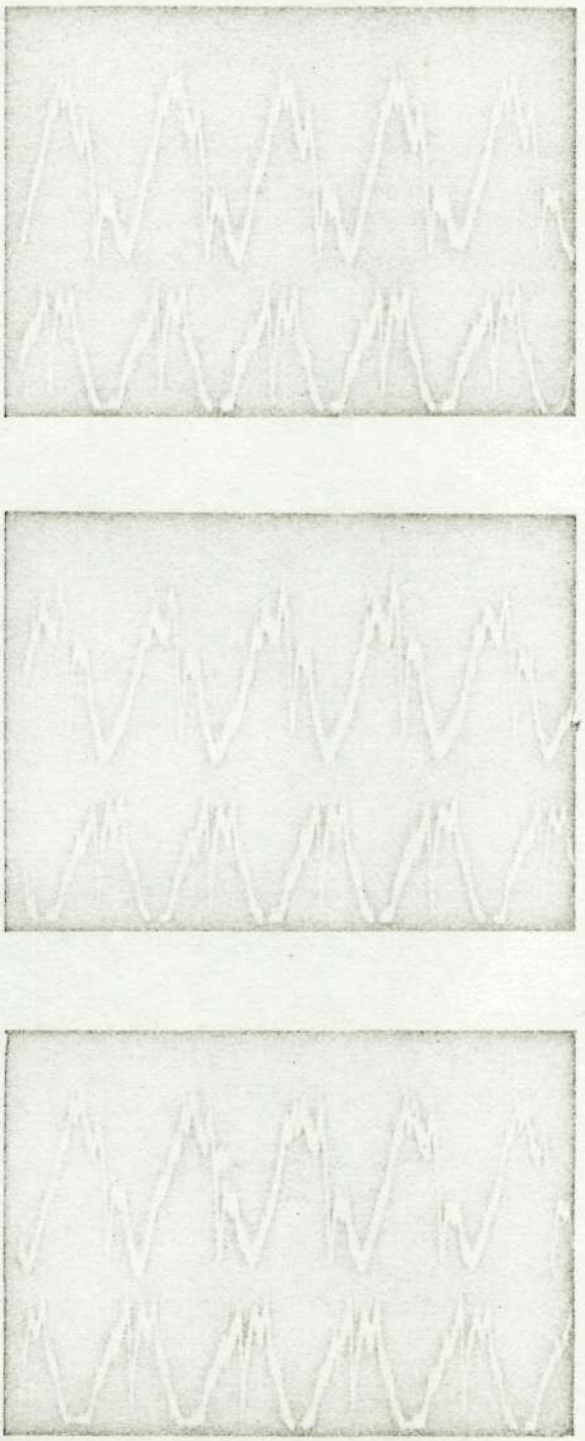

NOTE: Top trace in each photo is -SRA bearing; sweep is 0.02 second.

Fig. 21. Milliwattmeter trace and retainer motion during flip disturbance.

(Sheet 2 of 2)

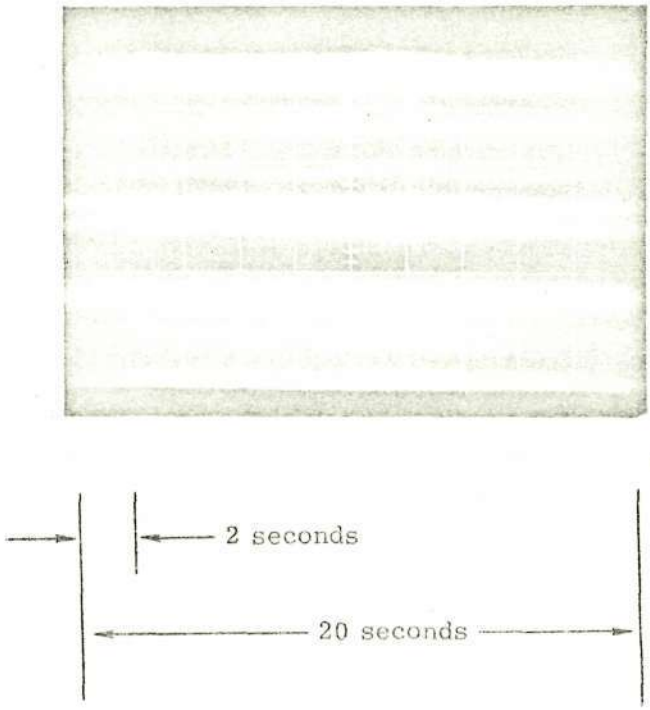

Fig. 22. Bearing-bearing interaction – stability.

heard also every 8 seconds. This is the only case where a bearing-bearing interaction has been found to influence Apollo retainer stability.

One very interesting and unexpected bearing-bearing effect in this same assembly is illustrated in Fig. 23, which shows seven of the small jags of Fig. 21 to the same time and torque scales. All eight occur at the same location on the torque sinusoid, meaning that the + SRA bearing produced a jag only when the two retainers were in the same relative position. A mechanism whereby an oil drop on retainer I would know where retainer II was relative to it is as follows: the drop leaves I when the centrifugal force on it is sufficiently large. If I is whirling slowly relative to its ball group, then the distance to the oil drop from the spin axis (hence the centrifugal field on it) will have a maximum once each relative rotation. If the drop grows slowly compared to this relative rotation, it will be most likely to fly off at those times when the field is maximized. Since a retainer whirls slowly relative to its ball group in phase with the ball

group in the other bearing, as a result of a bearing-bearing misalignment interaction, we have the desired mechanism. A difficulty in applying this explanation to Fig. 23 is that it was decided on the basis of ball-group-rate measurements that the jags must be in the + SRA bearing, but the probe outputs shown in Fig. 21 (and many more similar photos as well) indicate that the + SRA retainer is not whirling (or cocking) with respect to its ball group. We are unable to resolve the conflict at present.

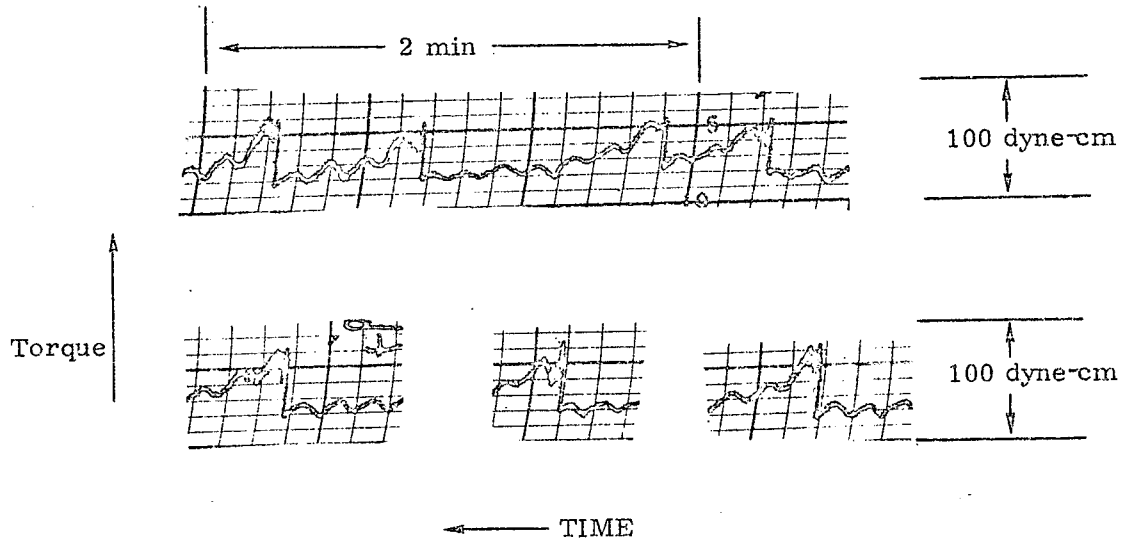

Fig. 23. Bearing-bearing interaction – jags.

APPENDIX

Approved: Albert P. Freeman
Albert P. Freeman
Deputy Associate Director
Charles Stark Draper Laboratory

Approved: David G. Hoag 28 Mar 72
David G. Hoag, Director
Apollo Guidance and
Navigation Program

Approved: Ralph R. Ragan
Ralph R. Ragan
Deputy Director
Charles Stark Draper Laboratory

E-2648

CROSS FLOW IN A STARVED EHD CONTACT

by

Edward P. Kingsbury

March 1972

To be presented at the ASLE Annual Meeting
in Houston, Texas, May 1-4, 1972.

ACKNOWLEDGMENT

This paper was prepared under the auspices of DSR Project 55-23829, which is sponsored by the Manned Spacecraft Center of the National Aeronautics and Space Administration through Contract NAS 9-4065.

Publication of this report does not constitute approval by NASA of the findings or conclusions contained herein. It is published for the exchange and stimulation of ideas.

E-2648

CROSS FLOW IN A STARVED EHD CONTACT

ABSTRACT

It is suggested that fluid film thickness in a starved EHD contact is determined by the rate at which lubricant is forced from the Hertz zone normal to the rolling direction. A simple model allows calculation of this flow rate, together with related quantities of interest to the designer.

by
Edward P. Kingsbury
March 1972

APPENDIX
TABLE OF CONTENTS

APPENDIX

LIST OF ILLUSTRATIONS

APPENDIX NOMENCLATURE

Symbol	Units	Definition
A, B, C, D		constants
E	in.	pitch diameter
F		$\left[\frac{1}{2}\ln\frac{(K+H)^2}{(K^2-KH+H^2)}+\sqrt{3}\tan^{-1}\left(\frac{2H-K}{K\sqrt{3}}\right)\right]$
H		h/h_o
K		$(-Q_{in}/Q_{out})^{1/3}$
L	in.	half length of Hertz zone
N	lbf	normal load carried by contact
P	$lbf/in.^3$	mean Hertz pressure
Q_{out} (in)	$in.^3/s$	flow out of (into) Hertz volume
T	s	real time
V	$in.^3$	Hertz half volume
Z		number of balls
d	in.	ball diameter
f		ratio between contact time and real time
h	in.	film thickness
t	s	contact time
w	in.	Hertz width
α	$in.^2/lbf$	pressure viscosity coefficient
μ	poise	viscosity
θ	rad	contact angle
Subscripts		
o		refers to conditions at t = 0
p		refers to conditions prior to t = 0
e		refers to conditions at t = ∞

E-2648

CROSS FLOW IN A STARVED EHD CONTACT

INTRODUCTION

The fundamental elastohydrodynamic problem is to calculate lubricant film thickness in a contact where elastic deformations have the same order of magnitude as the film thickness. Various solutions are available, falling into two types: a Grubin or "inlet" analysis, which solves Reynolds equation in the inlet up to the edge of the Hertz zone (1,2,3,4); and a "complete" analysis, involving simultaneous solution of the Reynolds and Hertz equations over the entire contact (5). In general any Grubin analysis ignores flows within the Hertz zone, and the available complete solutions are limited by mathematical complexity to a consideration of one-dimensional flow in the direction of rolling. Moreover, these solutions all suppose that film thickness is determined by parameters of load, speed, viscosity, geometry, and elasticity. The tacit assumption is made that thickness is not a function of the amount of lubricant, which is presumed to be present in excess at the contact. Attempts have been made to impose the effects of side leakage (e. g., 2) and oil supply limitation (e. g., 4) on the classical solutions. However, the modifications seem artificial and do not change the underlying theoretical model.

Considerable experience using ball bearings on the spin axis of precision gyroscopes has shown that successful operation can be obtained although the bearings are starved in an EHD sense. Starvation is defined as any operating condition such that an increase in oil available to the contact will result in an increase in film thickness (6). In this paper, starved EHD behavior is considered in several situations: when no new oil enters the contact, and when a step change in one of the rolling parameters is introduced at an equilibrium contact. Arguing that the important oil flow within the Hertz zone is across the rolling direction, one can formulate a simple theory which explains quantitatively some aspects of starved-ball-bearing behavior, e. g., the "oil jag."

OIL JAGS

An oil jag in a gyro spin-axis bearing is detected as an abrupt increase in driving torque demand, followed by a decay lasting over many seconds back to the original torque level (7,8). If the gyroscope is being accelerated perpendicular to its spin axis during the jag (spin axis and output axis horizontal), a simultaneous and one-one excursion, positive or negative depending upon which bearing of the pair is involved, is observed in its torque-to-balance signal (Fig. 1). This indicates an axial shift of the gyroscope CG.

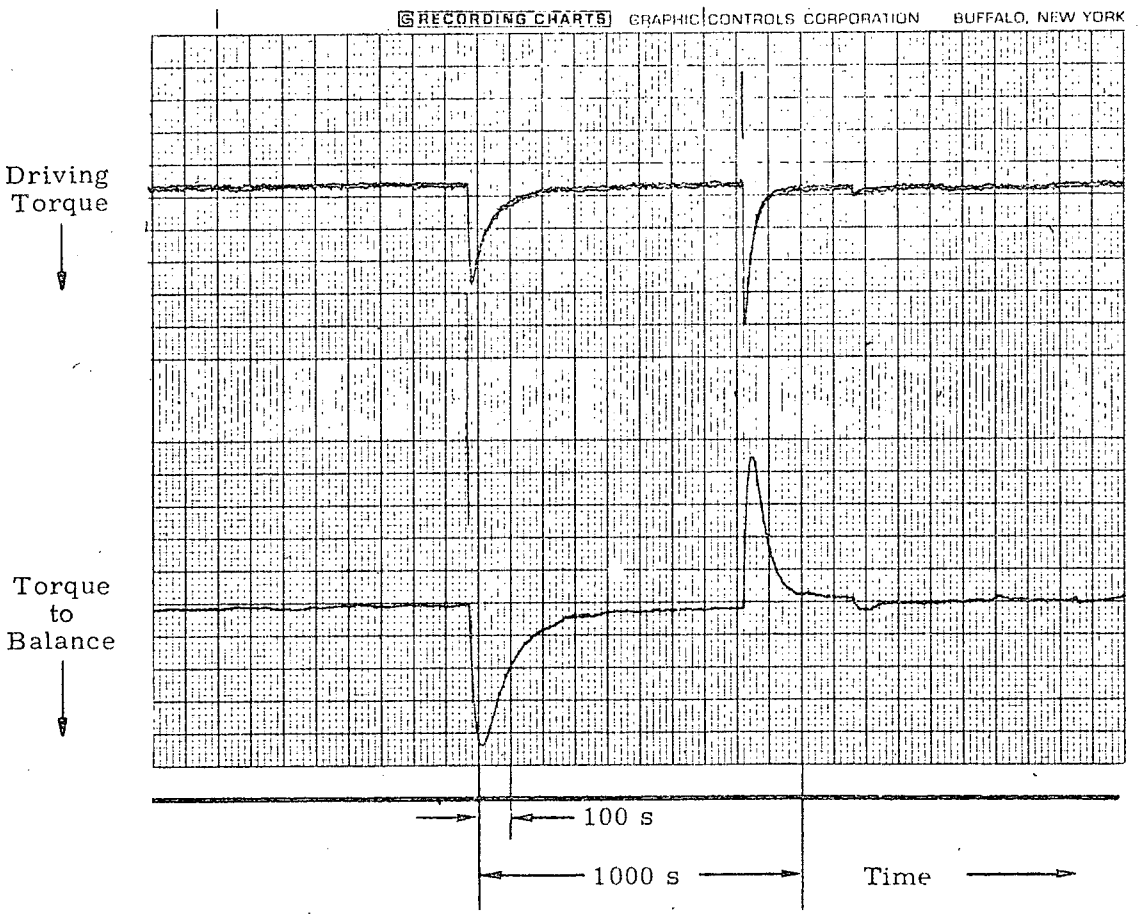

Fig. 1. Disturbances in driving torque and torque to balance during oil jag.

Suppose, in one ball retainer, that oil flows in the centrifugal field to its OD and accumulates in a droplet. The drop will grow to a cricital size determined by its surface tension and the field, whence it will fly off into the ball track. Energy required to roll the ball through the deepened oil is reflected in the driving torque excursion, and an axial shift of the gyro CG due to the increased film thickness in one bearing produces the torque-to-balance excursion (Fig. 2).

Various other jag observations are explained by this model; stroboscopic observation has confirmed oil droplets on the retainer OD, together with a torque excursion upon their disappearance; artificial jags have been produced with a "jag-gun" which throws a known amount of oil into the ball track on demand. Thus the model appears correct, and associates a known increase in film thickness with a known increment in the amount of oil available to the contact. Further, it gives the time required to reduce the film back to its original thickness.

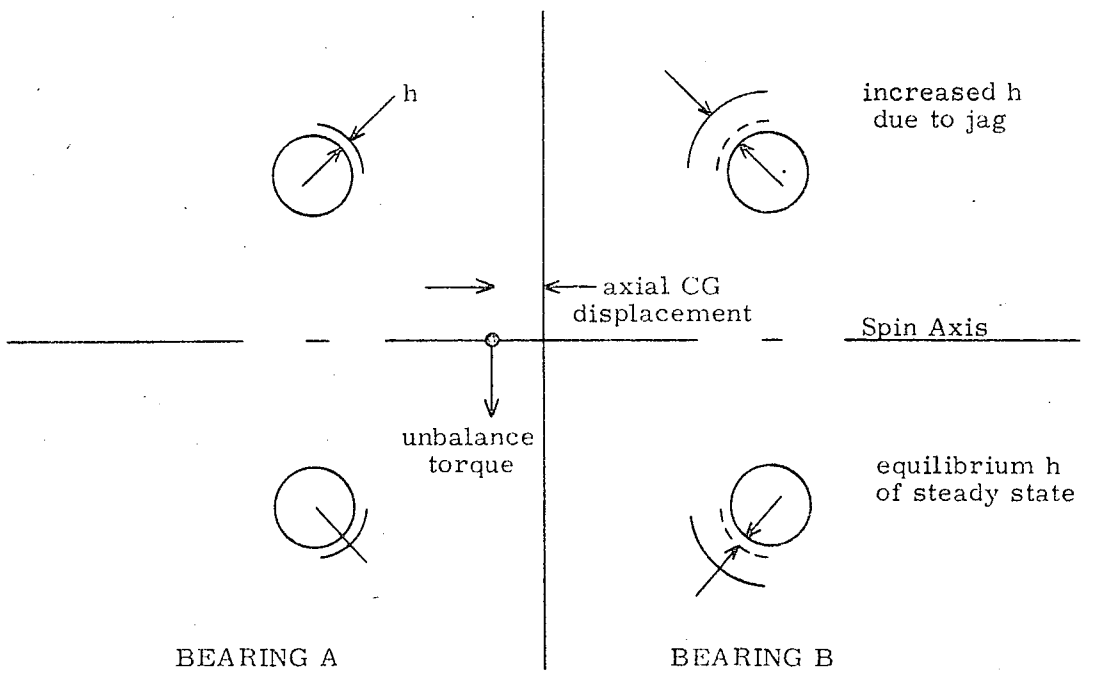

Fig. 2. Oil-jag-mechanism geometry.

FLOW MODEL FOR A STARVED CONTACT

In a starved bearing, the oil on the track is about as thick outside the contact as in it. Stroboscopic observation of interference fringes confirms that films so thin flow very slowly in the centrifugal fields due to bearing rotation. The working oil is thus stationary with respect to the track outside the contact and is unloaded most of the time. The oil momentarily in the contact may flow in the direction of rolling and also across the direction of rolling under the Hertz pressure acting on it. Its viscosity will be greatly increased while it is under this pressure. Flow in the rolling direction cannot alter the average film thickness since it removes no oil from the track. Only transverse oil flow can change the film thickness. The long-term decays in thickness observed with oil jags thus imply that transverse oil flow out of the Hertz zone should be considered in a starved EHD contact.

To estimate this outflow, approximate the volume of oil in each half of the Hertz zone at any time as (Fig. 3)

$$V = L\, w\, h \qquad [1]$$

where L and w are the Hertz dimensions of the contact, and h is the film thickness. Calculate the oil flow out each end of this box due to a pressure drop equal to the mean Hertz pressure, P, of an oil of viscosity $\mu = \mu(P)$ as

$$Q = \frac{P\, h^3\, w}{12\, \mu\, L} \qquad [2]$$

Flow in the roll direction may be neglected as it must average to zero.

$$dV = L\, w\, dh = -\, Q dt \qquad [3]$$

$$\frac{12\, \mu\, L^2}{P} \int \frac{dh}{h^3} = -\int dt + D \qquad [4]$$

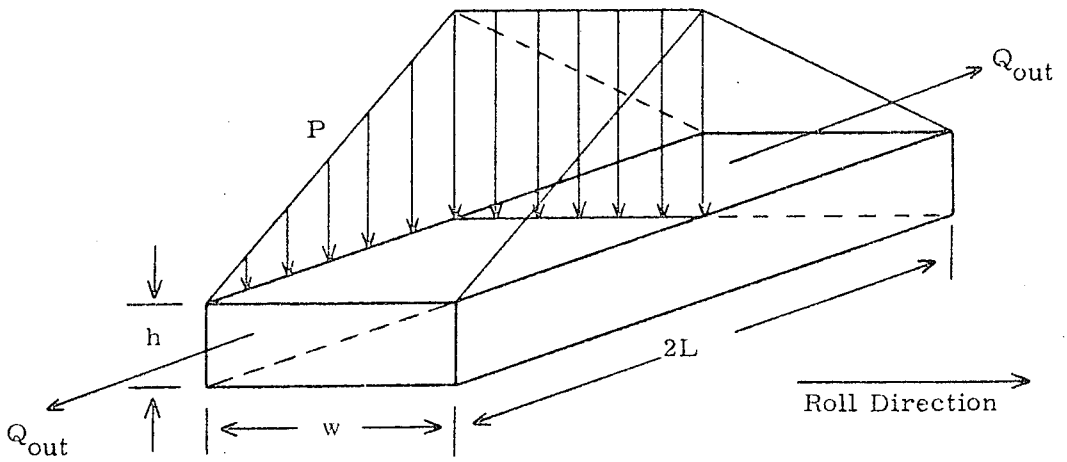

Fig. 3. Oil-film geometry in Hertz zone.

where t is the time an element in the race track is in the contact. It is a fraction f, of real time T, given by the proportion between Zw, the total contact width, and π (E + d cos B), the outer-race-track circumference. Thus,

$$t = fT,\ f = Zw/(E + d \cos\ \theta)\pi \qquad [5]$$

written for an outer-race contact in a bearing having Z balls of diameter d, pitch diameter E, and contact angle B.

Finally,

$$\frac{h}{h_o} = \left[\frac{h_o^2\ Pf}{6\ \mu\ L^2}\ T + 1\right]^{-1/2} \qquad [6]$$

which relates the decay of a film of original thickness h_o to real time T in a bearing where no new oil enters the wear track.

This calculation has been carried out for the R3-size bearing (Fig. 4) which produced the jags shown in Fig. 1. The results for two running conditions are plotted in Fig. 5. It takes about three hours of real-time running to pump half the oil out of a contact initially 20 x 10^{-6} inches thick under 150,000 lbf/in.^{2}. When the contact is 4 x 10^{-6} inches thick, it takes about 100 hours to pump out half the remaining

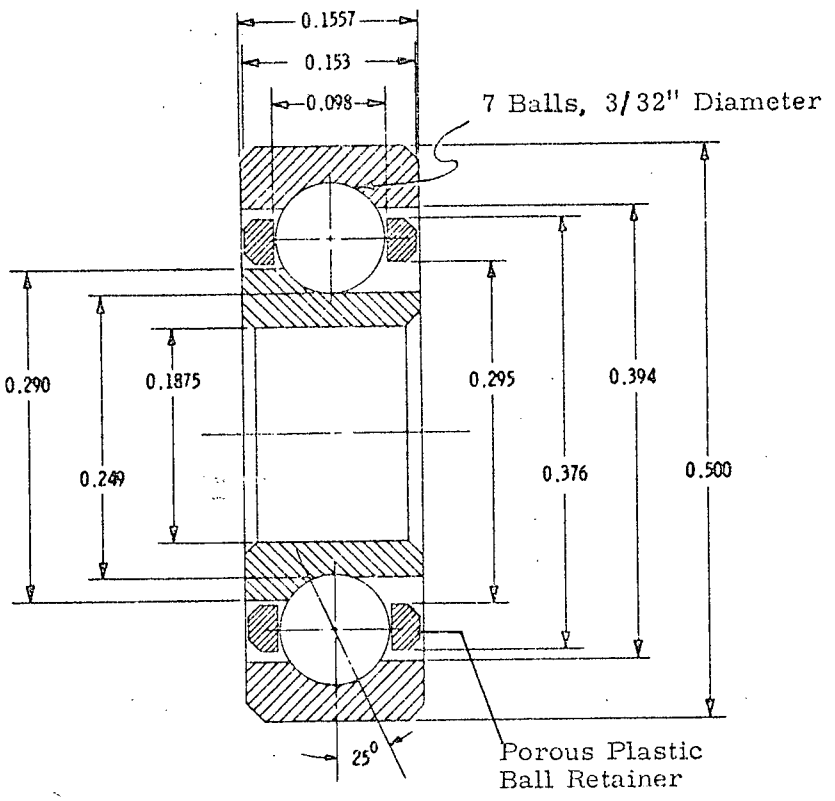

Fig. 4. R3 ball bearing.

oil. These numbers are not out of line with life experienced in retainerless bearings which have no provision for the recirculation of oil.

If the decay is recalculated for a Hertz stress of 100,000 lbf/in.^{2}, there is a decrease in the life of the contact. This is because of the very great decrease in the viscosity of the lubricant with pressure, from 10^6 to 10^4 poise in this case (9).

THE STARVED EQUILIBRIUM CONTACT

Since it is possible to run starved gyro bearings essentially indefinitely (10), there must be a flow of lubricant into the wear track to balance the outflow calculated in the preceeding section. It has been confirmed experimentally (11) that oil circulates from a reservoir in the ball retainer to the track and back, although the

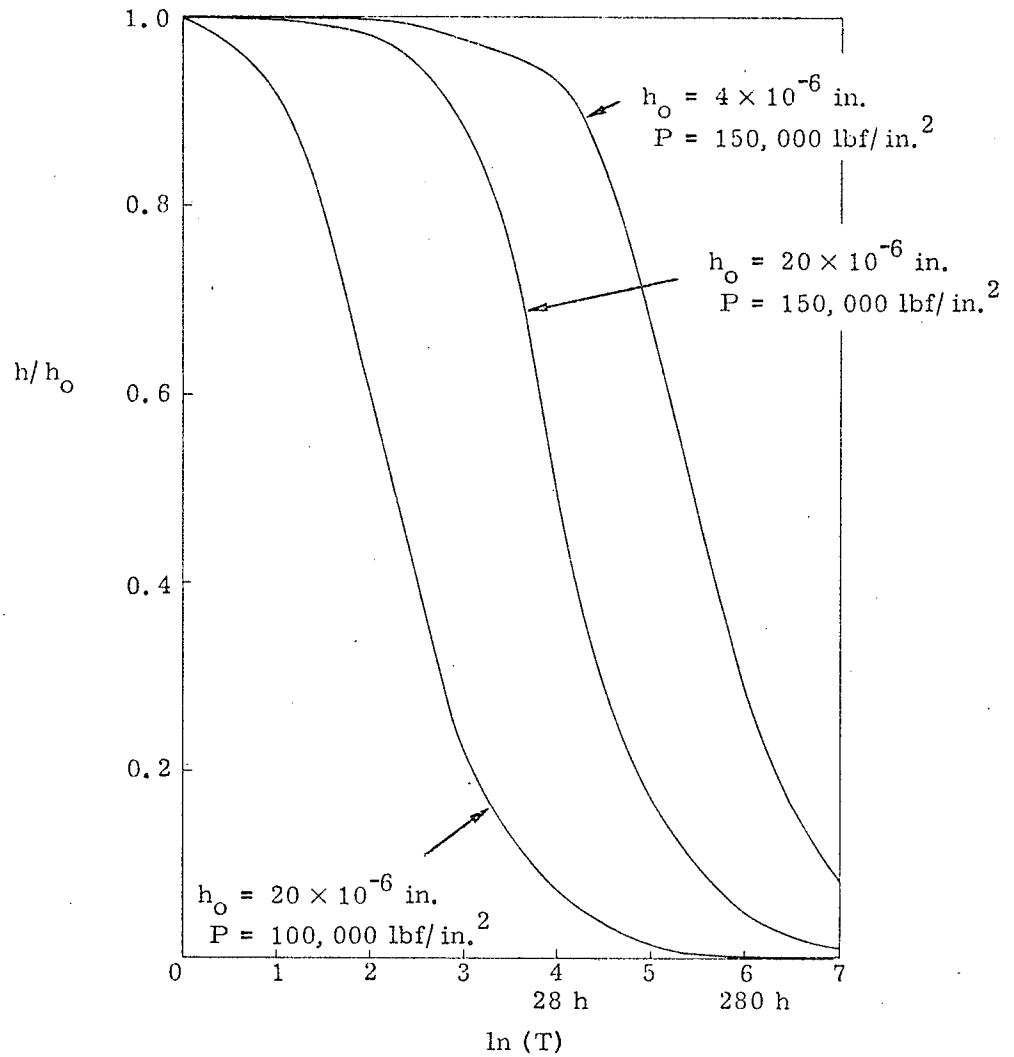

Fig. 5. Film decay without inflow.

details of the process have not been explored. At equilibrium, therefore, there is an inflow equal to the transverse outflow, and an equilibrium film thickness. If equilibrium is disturbed by a change in some running condition, the transient response in film thickness at the contact may be calculated.

In the following analysis, a step change is assumed to occur at $t = 0$; subscript p refers to equilibrium conditions prior to the change ($t < 0$); subscript o to conditions at the change ($t = 0$); and subscript e to final equilibrium ($t = \infty$).

Thus, at an equilibrium contact for $t < 0$

$$Q_{in\ p} = Q_{out\ p} = \frac{P_p w_p h_p^3}{12 \mu_p L_p} = Q_{in} \qquad [7]$$

It is supposed that the inflow to the contact, Q_{in}, is constant throughout the transient, since it is the result of long-term averaging processes in the retainer, but that the outflow steps at $t = 0$ since it depends directly on contact conditions. For $t \geq 0$

$$\frac{dV}{dt} = \frac{d}{dt}\left[L_o w_o h(t)\right] = Q_{in} - Q_{out}(t) \qquad [8]$$

$$Q_{out}(t) = \frac{P_o w_o h^3(t)}{12 \mu_o L_o} \qquad [9]$$

so that

$$12 \mu_o L_o^2 w_o \int_{h_o}^{h} \frac{dh}{12 \mu_o L_o Q_{in} - P_o w_o h^3} = \int_0^t dt \qquad [10]$$

Equation [10] may be integrated to get

$$\frac{L_o w_o h_o}{3 Q_{in}} K \left[F(H,K) - F(1,K)\right] = t \qquad [11]$$

where

$$K^3 = -\frac{Q_{in}}{Q_{out_o}}, \quad H = h/h_o$$

and

$$F(H,K) = \left[\frac{1}{2} \ln \frac{(K + H)^2}{(K^2 - KH + H^2)} + \sqrt{3} \tan^{-1}\left(\frac{2H - K}{K\sqrt{3}}\right)\right] \qquad [12]$$

F(H,K) has been plotted in Fig. 6 for relevant values of H and K.

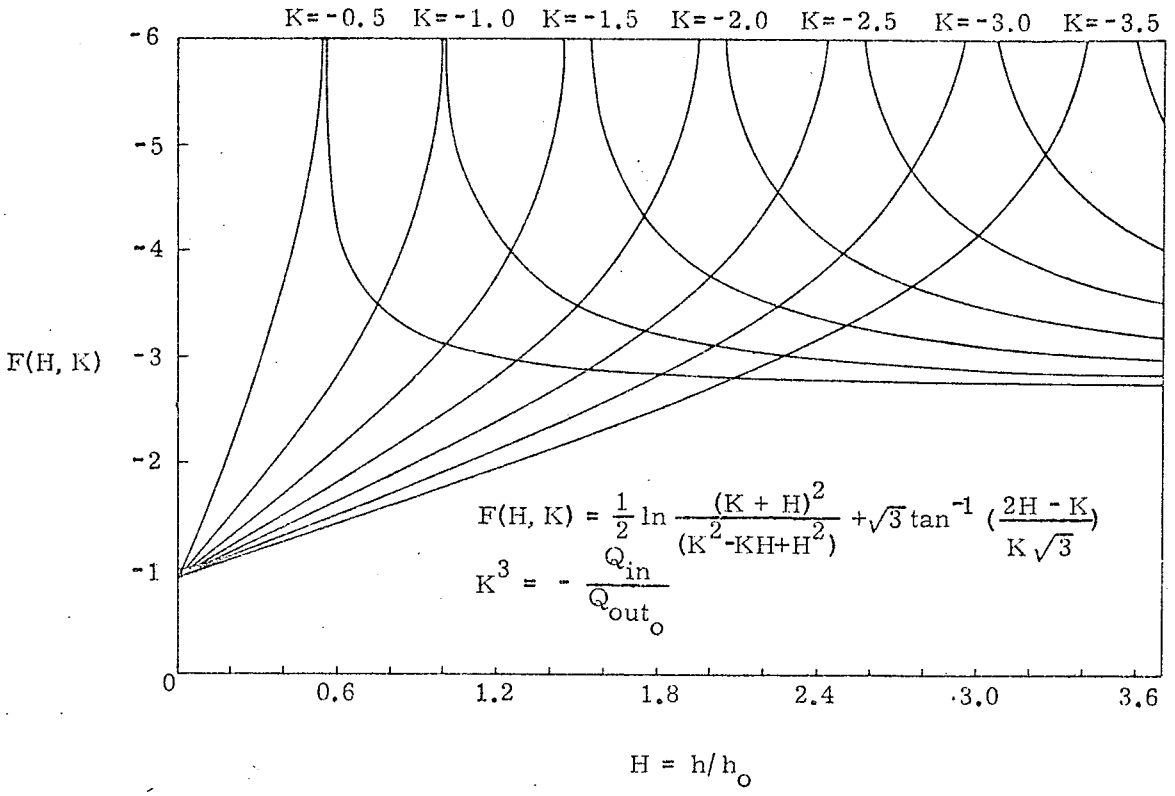

Fig. 6. F(H,K) versus H.

FILM-THICKNESS STEP

An oil jag may be simulated as a step increase in film thickness from h_p to h_o, all other running parameters remaining constant. Then, from Eq. [12]

$$\frac{h_p}{h_o} = H_p = |K| < 1 \qquad [13]$$

Suppose $H_p = +0.5$, meaning that the bearing jags to a new thickness twice the prior equilibrium value. Equation [11] becomes

$$-0.5\left(\frac{L_o w_o h_o}{Q_{in}}\right)[F(H, -0.5) - F(1, -0.5)] = t \qquad [14]$$

Boundary conditions are satisfied since at $t = 0$

$$F(H_o, -0.5) = F(1, -0.5),\ H_o = 1 \text{ and } h = h_o \qquad [15]$$

and at $t = \infty$, $F(H_e, -0.5) = -\infty$ occurring (Fig. 6) when $H_e = -K$ or

$$0.5 = H_e = h_e/h_o,\ h_e = 1/2\ h_o \qquad [16]$$

Thus, for this case Eq. [11] describes a time decay from the stepped film thickness at $t = 0$ back to the prior equilibrium thickness at $t = \infty$.

As a numerical example, suppose an R3 bearing ($F = 0.01$) is running on an equilibrium film $h_p = 20 \times 10^{-6}$ inches thick, with a Hertz pressure $P_p = 10^5$ lbf/in.^{2}, and oil viscosity $\mu = 1.1 \times 10^4$ poise. At $t = 0$ the bearing jags to $h_o = 24 \times 10^{-6}$ inches, giving a K value of $-\frac{20}{24} = -0.833$. Using Fig. 6 and Eq. [11], the decay shown in Fig. 7 is calculated. It may be compared with jags experienced in similar bearings (Fig. 1).

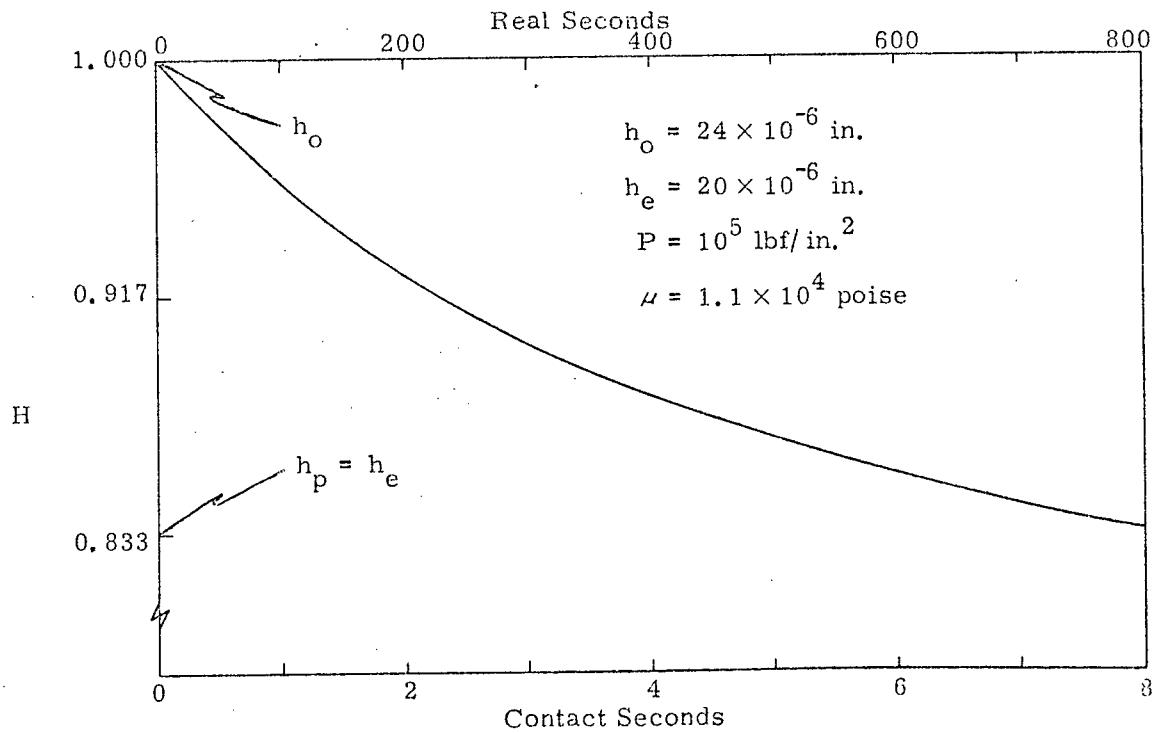

Fig. 7. Film decay after jag.

LOAD STEP

Suppose that at $t = 0$ the load carried at a starved EHD contact steps from N_p to N_o. From elasticity theory

$$(P, w, L) = (A, B, C)N^{1/3} \qquad [17]$$

where A, B, and C are constants which may be calculated according to the particular bearing under consideration.

Assume an exponential dependence of viscosity on pressure, as is done in Ref. (4):

$$\mu_o = \mu_p e^{\alpha(P_o - P_p)} = \mu_p^{A\alpha(N_o^{1/3} - N_p^{1/3})} \qquad [18]$$

Thus, at the load step, the Hertz pressure, the Hertz dimensions, and the viscosity all change to new values. However, the thickness does not step, $h_p = h_o$. Its time dependence for $t > 0$ is given by Eq. [11]. From Eq. [12]

$$K^3 = -\frac{Q_{in}}{Q_{out_o}} = -\frac{P_p w_p L_o \mu_o}{P_o w_o L_p \mu_p} \qquad [19]$$

or, in terms of load

$$K^3 = -\left(\frac{N_p}{N_o}\right)^{1/3}\left[e^{A\alpha(N_o^{1/3} - N_p^{1/3})}\right] \qquad [20]$$

The exponential part of K ensures that $|K| > 1$, meaning that H values will be found on the left branch of the F curves in Fig. 6. To calculate the final equilibrium film thickness, note that at $t = \infty$, $-F(H,K) = \infty$. From Fig. 6

$$-K = H_e, \quad h_e = h_o |K| \qquad [21]$$

h_e may also be calculated by observing that at $t = \infty$, $Q_{out_e} = Q_{in}$. Substitution gives the same result for h_e.

For this case, Eq. [11] thus describes a build-up in film thickness with time after a step increase in load (Fig. 8).

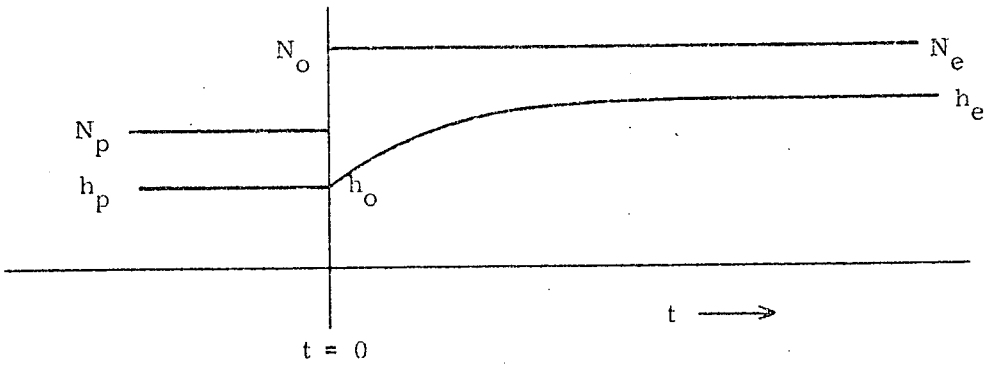

Fig. 8. Film thickness history after load step.

DISCUSSION

This analysis indicates that to calculate the EHD film thickness in a starved contact, it is necessary to know the rate at which lubricant is supplied to the contact. In a conventional instrument bearing, oil is stored in the ball retainer and metered out by unknown processes at unknown rates at the different ball pockets. The direct calculation of film thickness in these bearings is therefore not feasible.

Testing of retainerless bearings which incorporate a rational lubrication supply system has been started. The oil supplies for these bearings have been specifically designed to provide well-defined inflows. As such information becomes available, thickness predictions from the cross-flow analysis can be tested.

The model for cross flow is crude but is believed to reflect some reality. Calculation of life and jag decay seems adequate, and special experiments to check some other predictions are under consideration. Predictions include independence of jag decay period with speed, and increase in decay period with stress. Depending on the outcome of such experiments, this model can be improved or scrapped.

APPENDIX REFERENCES

1. Grubin, A. N., and Vinogradova, I. E., Book No. 30, Central Scientific Research Institute for Technology and Mechanical Engineering, Moscow, 1949.
2. Archard, J. F., and Cowking, E. W., "A Simplified Treatment of Elastohydrodynamic Lubrication Theory for a Point Contact," Lubrication and Wear, Group Symposium on Elastohydrodynamics Lubrication, Paper 3, Institution of Mechanical Engineers, London, 1965.
3. Cheng, H. S., "A Numerical Solution of the Elastohydrodynamic Film Thickness in an Elliptical Contact," ASME paper # 69-LUB-17.
4. Wedeven, L. D., Evans, D., and Cameron, A., "Optical Analysis of Ball Bearing Starvation," Trans., ASME, JOLT 93F, No. 3, 1971.
5. Dowson, D. and Higginson, G. R., Elastohydrodynamic Lubrication, Pergamon Press, London, 1966.
6. Kingsbury, E. P., "Experimental Observations on Instrument Ball Bearings," Bearing Conference Proceedings, Dartmouth College, Hanover, New Hampshire, 1968.
7. Archibald, F. R., and Blasingame, B. P., "The Jag Mechanism in Gyroscopes," Air, Space and Instruments, McGraw-Hill, 1963.
8. Horsch, J. D., "Correlation of Gyro Spin-Axis Ball Bearing Performance with the Dynamic Lubricating Film," ASLE Trans., 6, 112, 124 (1963).
9. ASME Pressure-Viscosity Report, ASME, New York, 1953.
10. Freeman, A. P., "Gyro Ball Bearings – Technology Today," presented at 6th AGARD Guidance & Control Meeting, "Inertial Navigation: Components," Braunschweig, Germany, 1968.
11. Roberts, M., A Study of Oil Circulation in the R4 Spin-Axis Bearing with Sintered Nylon Ball Retainers, MIT/DL Report E-2082, Cambridge, Mass. (1966).

LIST OF REFERENCES

1. Kingsbury, E. P., Oil Film Parameter Investigation, Charles Stark Draper Laboratory Report C-3703, December 1970.

2. Hertz, H., Miscellaneous Papers, The Macmillan Co., N.Y., 1896.

3. Wedeven, L. D., D. Evans, and A. Cameron, "Optical Analysis of Ball Bearing Starvation," Trans., ASME, JOLT 93F, No. 3, 1971.

4. Wedeven, L. D., Surface Tension Measurement in Air of Liquid Lubricants to 200°C by the Differential Maximum Bubble Pressure Technique, NASA TN D-6450, September 1971.

5. Kingsbury, E. P., "Fluid State in the Inlet Region," Tribology 2, No. 4, 1969.

6. Bickerman, J., Surface Chemistry, Academic Press, N.Y., 1958.